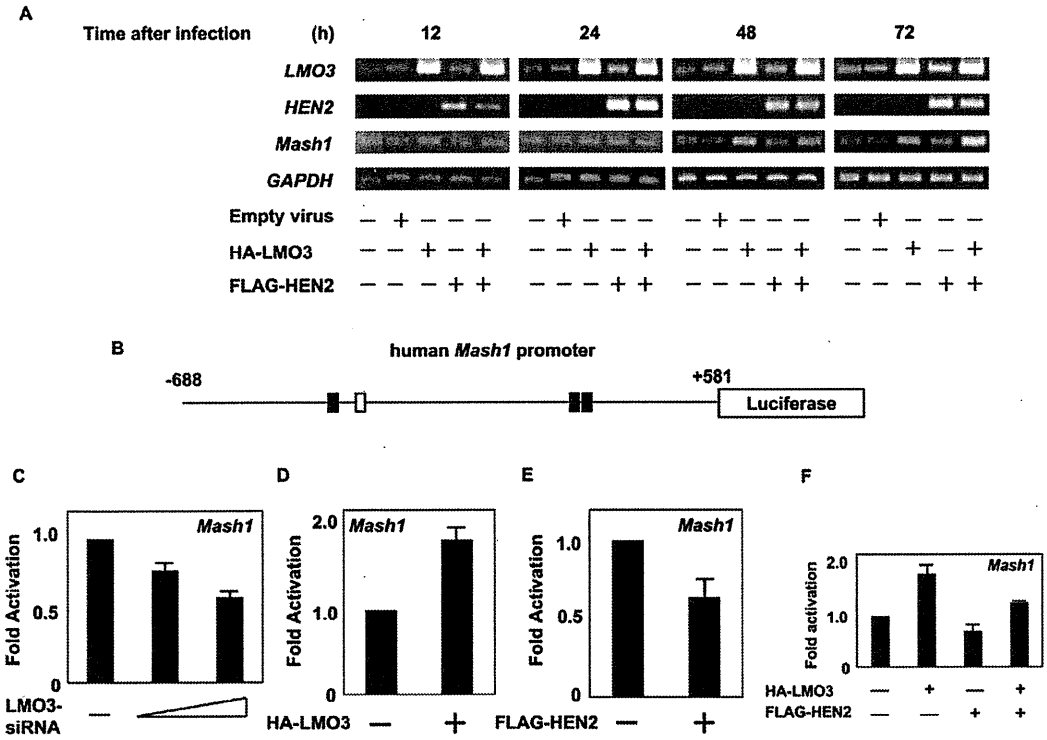


**Figure 3. LMO3/HEN2-mediated transcriptional induction of *Mash1*.** (A) RT-PCR. SH-SY5Y cells were infected with empty adenovirus or with the indicated combinations of recombinant adenovirus encoding HA-LMO3 or FLAG-HEN2. At the indicated time points after infection, total RNA was analyzed for expression levels of *LMO3*, *HEN2* and *Mash1* by RT-PCR. *GAPDH* was used as an internal control. (B) Schematic drawing of human *Mash1* promoter. Nucleotide positions were indicated relative to transcriptional initiation site (+1). The putative HES1-binding sites and E-box were depicted by filled and open boxes, respectively. This genomic fragment was subcloned into appropriate restriction sites of pGL3-Basic Vector to give pluc-hMash1. (C) siRNA-mediated knockdown of LMO3 reduces the promoter activity of *Mash1*. SH-SY5Y cells were co-transfected with constant amount of pluc-Mash1 (100 ng) and pRL-CMV (0.2 ng) in the presence or absence of increasing amounts of expression plasmid for siRNA against human LMO3 (100 or 400 ng). Forty-eight hours after transfection, cells were lysed and their luciferase activities were measured. (D) LMO3 transactivates *Mash1* promoter. Mouse neuroblastoma Neuro2a cells ($1 \times 10^5$ cells/24-well plate) were co-transfected with constant amount of pluc-hMash1 (100 ng) and pRL-CMV (0.2 ng) together with or without expression plasmid for HA-LMO3 (150 ng). Forty-eight hours after transfection, cells were lysed and their luciferase activities were measured. (E) HEN2 inhibits *Mash1* promoter activity. Luciferase activities were measured in Neuro2a cells with or without FLAG-HEN2 (100 ng). (F) LMO3 interferes with negative effect of HEN2 on Mash1 transcription in Neuro2a cells. Luciferase activities were measured in Neuro2a cells transfected with HA-LMO3 (150 ng), FLAG-HEN2 (100 ng) or both of them.
doi:10.1371/journal.pone.0019297.g003

To ask about mechanistic insights into understanding how LMO3 and/or HEN2 could attenuate the inhibitory effects of HES1 on *Mash1* expression, we performed chromatin immunoprecipitation (ChIP) assay. Similar to human *Mash1* promoter, mouse *Mash1* promoter also contains three putative HES1-binding sites and one E-box (Figure 4C). Neuro2a cells were transfected with constant amount of empty plasmid or with expression plasmid for Myc-HES1 together with or without increasing amounts of FLAG-HEN2 expression plasmid. Forty-eight hours after transfection, cross-linked chromatin was prepared and subjected to ChIP assay. As shown in Figure 4D, the anti-Myc tag immunoprecipitates contained genomic fragments including putative HES1-binding sites as well as E-box. The amounts of Myc-HES1 recruited onto HES1-binding sites and E-box significantly decreased in the presence of FLAG-HEN2 in a dose-dependent manner. Additionally, the anti-FLAG immunoprecipitates contained genomic fragments including putative HES1-binding sites and E-box in the absence of exogenous HES1. Co-expression of FLAG-HEN2 and Myc-HES1 inhibited recruitment of FLAG-HEN2 onto putative HES1-binding sites and E-box, however, its inhibition was efficiently abrogated by increasing amounts of FLAG-HEN2. These results suggest that HEN2 might compete with HES1 in binding to putative HES1-binding sites and E-box, and thereby inducing the expression of *Mash1*.

## HEN2 Interacts with HES1 in cells

To examine whether HEN2 could interact with HES1 in cells, we performed immunoprecipitation experiments. Cell lysates prepared from Neuro2a cells co-transfected with the indicated combinations of expression plasmids were subjected to immunoprecipitation. As clearly shown in Figure 5A, HES1 was co-immunoprecipitated with FLAG-HEN2. Consistent with these results, reciprocal experiments showed that the anti-Myc tag immunoprecipitates contain FLAG-HEN2. *In vitro* pull-down assay demonstrated that radio-labeled FLAG-HEN2 is co-immunoprecipitated with Myc-HES1 (Figure 5B). Additional immunoprecipitation experiments demonstrated that LMO3 also forms a stable complex with HES1 (Figure 6A). We have previously showed that LMO3 forms a stable complex with HEN2 [7]. To investigate the effect of LMO3 on binding of HEN2 and HES1 to putative HES1-binding sites and E-box,

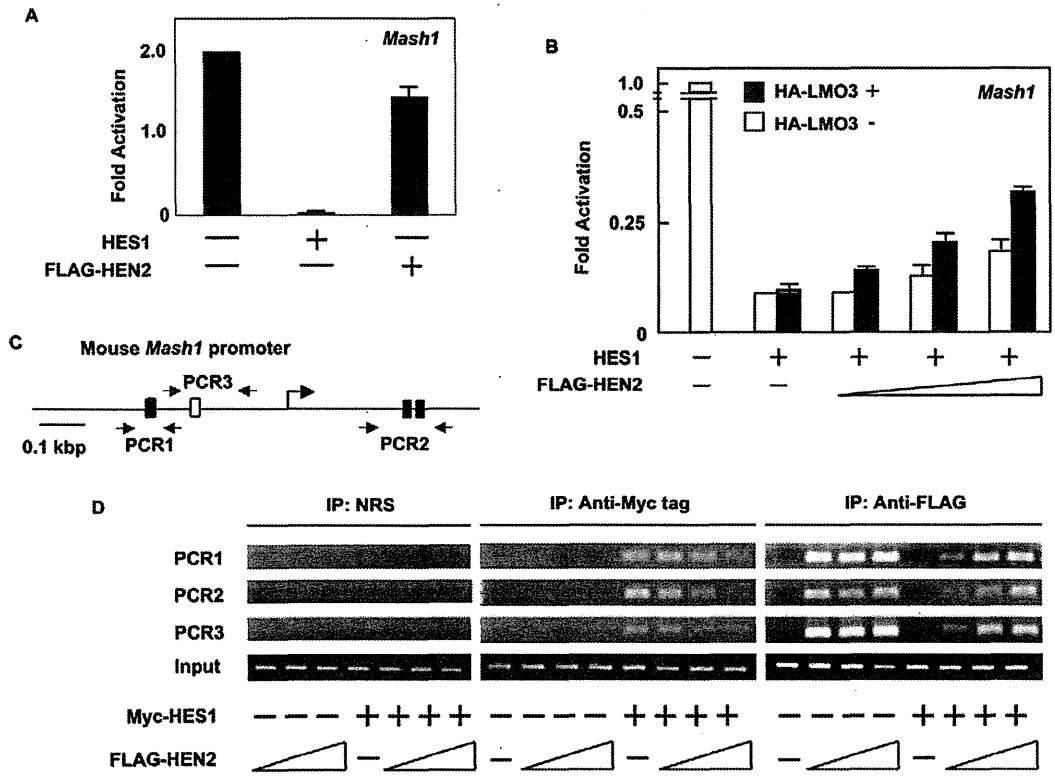


**Figure 4. LMO3/HEN2 attenuates HES1-dependent down-regulation of *Mash1*.** (A) Luciferase reporter assay. Neuro2a cells were co-transfected with constant amount of pluc-hMash1 (100 ng), pRL-CMV (0.2 ng) and expression plasmid for HES1 (50 ng) or HEN2 (50 ng). Forty-eight hours after transfection, cells were lysed and their luciferase activities were examined. (B) Luciferase reporter assay. Neuro2a cells were co-transfected with constant amount of pluc-hMash1 (100 ng), pRL-CMV (0.2 ng) and expression plasmid for HES1 (5 ng) in the presence or absence of expression plasmid for HA-LMO3 (150 ng) together with or without increasing amounts of FLAG-HEN2 expression plasmid (100, 200 or 300 ng). Forty-eight hours after transfection, cells were lysed and their luciferase activities were examined. (C) Schematic representation of mouse *Mash1* promoter. The canonical HES1-binding sites and E-box were indicated by filled and open boxes, respectively. The positions of primer sets used for chromatin immunoprecipitation (ChIP) assays were also indicated. (D) ChIP assay. Cross-linked chromatin prepared from Neuro2a cells transfected with the indicated combinations of expression plasmids was sonicated and immunoprecipitated with normal rabbit serum (NRS), polyclonal anti-Myc tag or with polyclonal anti-FLAG antibody. The genomic DNA was purified from the immunoprecipitates and amplified by PCR.
doi:10.1371/journal.pone.0019297.g004

Neuro2a cells were transfected with Myc-HES1 or FLAG-HEN2 together with or without HA-LMO3 expression plasmid and subjected to ChIP assay. As shown in Figure 6B, the immunoprecipitates using anti-Myc tag or anti-FLAG tag antibody contained genomic fragments including putative HES1-binding sites as well as E-box. The amount of Myc-HES1 recruited onto HES1-binding sites and E-box decreased in the presence of HA-LMO3. On the other hand, the amount of FLAG-HEN2 recruited onto HES1-binding sites and E-box increased in the presence of HA-LMO3. As shown in Figure 3F, LMO3 interferes with inhibitory effect of HEN2 on Mash1 expression. These suggest that LMO3 may additively interfere with the inhibitory effect of HES1 on *Mash1* expression by promoting binding of HEN2 to HES1-binding sites and E-box. Collectively, it is conceivable that LMO3/HEN2 reduces the inhibitory effect of HES1 on *Mash1* expression through binding to HES1 and thereby blocking its recruitment onto putative HES1-binding sites and E-box (Figure 7 and Figure S3).

## Discussion

In this study, we found that *Mash1* is one of transcriptional targets of LMO3/HEN2 transcriptional complex, and its protein product may play an important role in regulation of neuroblastoma cell growth. As described previously [14], *HEN1* as well as its closely related gene *HEN2* encodes bHLH-type transcription factor, which might recognize E-box (5′-CACGTG-3′). On the other hand, HES1 has an intrinsic transcriptional repressor activity [10]. Based on our present results, adenovirus-mediated expression of LMO3/HEN2 significantly induced *Mash1*, and HES1-mediated down-regulation of *Mash1* promoter activity was recovered by co-expression of LMO3 and HEN2. Our ChIP analyses indicated that HES1 binds to HES1-recognition sites and E-box within *Mash1* promoter in the absence of HEN2, whereas HEN2 efficiently inhibits the recruitment of HES1 onto HES1-binding sites and E-box within *Mash1* promoter, suggesting that HES1 occupies HES1-binding sites and E-box to inhibit the promoter activity of *Mash1*. On the other hand, HEN2 formed a complex with HES1 and reduced the amounts of HES1 recruited onto HES1-binding sites as well as E-box to increase the promoter activity of *Mash1* in collaboration with LMO3. Thus, it is likely that the balance between intracellular amounts of HES1 and LMO3/HEN2 might determine expression levels of *Mash1*, and thereby regulating neuroblastoma cell growth.

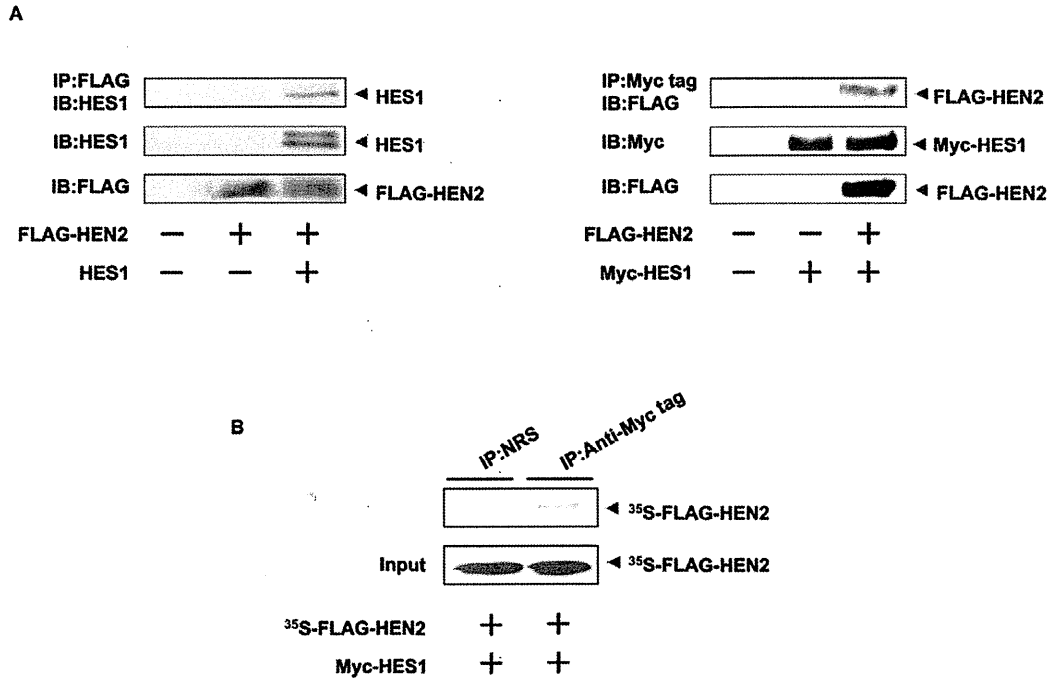


**Figure 5. Interaction between HEN2 and HES1 in cells.** (A) Neuro2a cells were co-transfected with the indicated combinations of expression plasmids. Forty-eight hours after transfection, cells were lysed and immunoprecipitated with anti-FLAG (left panel) or with anti-Myc tag antibody (right panel) and the immunoprecipitates were analyzed by immunoblotting with anti-HES1 or with anti-FLAG antibody, respectively. Aliquots of cell lysates were subjected to immunoblotting with anti-HES1, anti-FLAG or with anti-Myc tag antibody. (B) *In vitro* pull-down assay. Radio-labeled FLAG-HEN2 was incubated with cell lysates prepared from Neuro2a cells transfected with Myc-HES1 expression plasmid. The reaction mixture was immunoprecipitated with normal rabbit serum (NRS) or with polyclonal anti-Myc tag antibody and separated by SDS-PAGE followed by autoradiography. 1/5 inputs were also shown.
doi:10.1371/journal.pone.0019297.g005

It was reported that de-repression of *Mash1* might interfere with differentiation of sympatho-adrenal precursors of *Insm1* mutant mice although *Mash1* is expressed transiently in those cells during normal neural differentiation [15]. Furthermore, Watt et al. reported that N-myc positively regulates *Mash1* transcription [16]. Therefore, it is possible that in the transcriptional regulation of *Mash1*, LMO3 and HEN2 may associate with other nuclear factors like Insm1 and N-myc besides HES1.

From the developmental point of view, it is known that the LMO/HEN complex plays an important role in regulating neuronal differentiation [11,17]. As described [7,18], expression of *LMO3* was highly restricted in adult and fetal brains, and *HEN2* was expressed in developing nervous system. Genetic studies demonstrated that HEN2 participates in proper neural crest-derived neuroendocrine development and that Mash1 has a critical role in maintaining neuroendocrine cell phenotype [19,20]. Although *LMO3*-knockout mice did not exhibit any significant developmental defects, mice lacking both LMO1 and LMO3 died after birth, which might be due to neural defects [21]. Since neuroblastoma is one of the most common childhood solid tumors of peripheral nervous system arising from as yet unidentified population of neural crest cells [22] and Mash1 regulates proliferation of the sympathetic nervous system [23], it is likely that deregulated expression of Mash1 could contribute to genesis and development of neuroblastoma, which might be regulated by LMO3/HEN2 transcriptional complex both *in vitro* and *in vivo*. This LMO3/HEN2-HES1-Mash1 pathway could be the new future target for developing the anti-neuroblastoma treatment.

## Materials and Methods

### Ethics Statement

A hundred human neuroblastoma specimens used in the present study were kindly provided from various institutions and hospitals in Japan to the Chiba Cancer Center Neuroblastoma Tissue Bank. Written informed consent was obtained at each institution or hospital. This study was approved by the Chiba Cancer Center Institutional Review Board and were conducted according to the principles expressed in the Declaration of Helsinki.

### Tumor Specimens

Tumors were classified according to the International Neuroblastoma Staging System (INSS); 25 Stage 1, 13 Stage 2, 33 Stage 3, 23 Stage 4, and 6 Stage4s. Clinical information including age at diagnosis, tumor origin, Shimada's histology, prognosis, and survival months of each patient were obtained. The median follow-up time for survivors was 35 months (range 3 to 91 months). Each tumor specimen was assayed for *TRKA* expression by Northern blot analysis and for *MYCN* amplification status by both fluorescence in situ hybridization (FISH) and real-time quantitative polymerase chain reaction (PCR).

### Quantitative Real-time PCR

Total RNA prepared from primary neuroblastomas was reverse transcribed into cDNA (SuperScript II kit) and subjected to the real-time PCR. The expression level of *GAPDH* was measured in all samples to normalize *LMO3* and *Mash1* expression according to

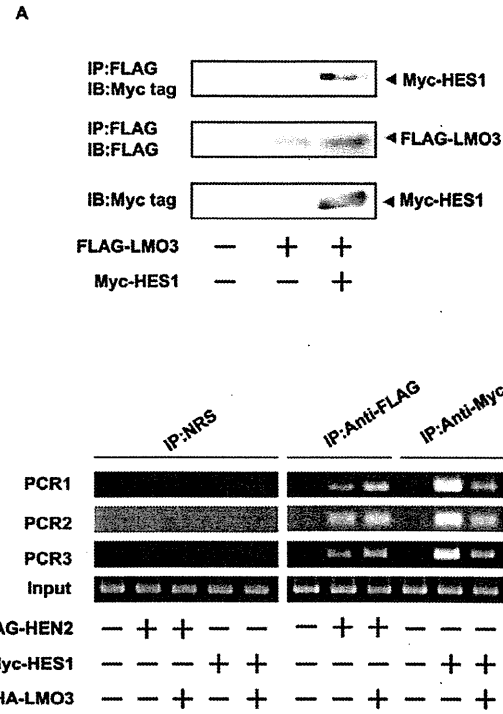


**Figure 6. LMO3 attenuates binding of HES1 to Mash1 promoter and promotes that of HEN2.** (A) Complex formation between LMO3 and HES1 in cells. Neuro2a cells were transiently transfected with the indicated combinations of the expression plasmids. Forty-eight hours after transfection, cell lysates were immunoprecipitated with anti-FLAG antibody followed by immunoblotting with anti-Myc tag antibody (top panel). Expressions of FLAG-LMO3 and Myc-HES1 are also shown (lower panels). (B) ChIP assay. Cross-linked chromatin prepared from Neuro2a cells transfected with the indicated combinations of expression plasmids was sonicated and immunoprecipitated with normal rabbit serum (NRS), polyclonal anti-Myc tag or with polyclonal anti-FLAG antibody. The genomic DNA was purified from the immunoprecipitates and amplified by PCR.
doi:10.1371/journal.pone.0019297.g006

the manufacturer's instructions (Applied Biosystems, Foster City, CA, USA). Oligonucleotide primers and TaqMan probes, which were labeled at the 5′ end with the reporter dye 6-carboxyfluorescein (FAM) and at the 3′ end with the quencher dye 6-carboxytetramethylrhodamine (TAMRA), were as follows: *LMO3*: forward 5′-TCTGAGGCTCTTTGGTGTAACG-3′, reverse 5′-CCAGGTGGTAAACATTGTCCTTG-3′ and probe 5′-FAM-AAACTGCGCTGCCTGTAGTAAGCTCATCC-TAMRA-3′. Taqman(R) Gene Expression Assay (Applied Biosystems) was purchased for *Mash1* with Assay ID Hs00269932-m1. Amplification and detection were done using the ABI Prism 7700 Sequence Detection System (Applied Biosystems).

## Statistical Analysis

Student's *t* tests were used to explore possible associations between *LMO3* expression and other factors. The distinction between high and low levels of *LMO3* and *Mash1* expression was based on the mean value. Kaplan-Meier survival curves were calculated, and survival distributions were compared using the log-rank test. Cox regression models were used to explore associations among *LMO3* expression, *Mash1* expression, age, *MYCN* amplification, tumor origin, Shimada classification and survival. Statistical significance was declared if $P<0.05$.

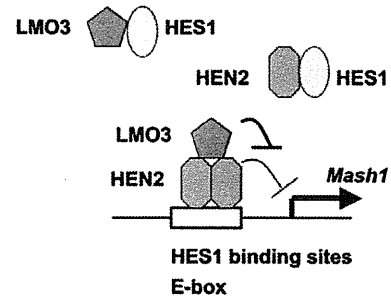


**Figure 7. Model for LMO3 and HEN2 cooperation in transcriptional regulation of Mash1 in Neuroblastoma.** HES1 binds to HES1 binding sites and E-box on *Mash1* promoter and represses *Mash1* transcription. LMO3 inhibits recruitment of HES1 onto HES1-binding sites and E-box on *Mash1* promoter by forming complex with HES1. HEN2 interferes with recruitment of HES1 onto HES1-binding sites and E-box on *Mash1* promoter by forming complex with HES1 and competing with HES1 in binding to these sites. LMO3 promotes recruitment of HEN2 onto HES1-binding sites and E-box on *Mash1* promoter by forming complex with HEN2 but inhibits negative effects of HEN2 on *Mash1* promoter. Thereby expression of *Mash1* is up-regulated.
doi:10.1371/journal.pone.0019297.g007

## Cell Culture and Transfection

SH-SY5Y (human neuroblastoma, ATCC number CRL-2266), SK-N-BE (human neuroblastoma, ATCC number CRL-2271) and Neuro2a (mouse neuroblastoma, ATCC number CCL-131) cells were maintained in RPMI 1640 supplemented with 10% heat-inactivated fetal bovine serum at 37°C in an atmosphere of 5% $CO_2$ in the air. Cells were transfected with the indicated expression plasmids using Lipofectamine 2000 transfection reagent (Invitrogen, Carlsbad, CA, USA) as recommended by the manufacturer.

## Generation of Recombinant Retroviral Vector and Retrovirus-mediated Gene Transfer

Human *Mash1* cDNA was subcloned into the *Hpa*I restriction site of the pLXSN vector. pLXSN or pLXSN- *Mash1* was transfected into the φ2 packaging cells, and SH-SY5Y cells ($1\times10^6$ cells) infected with virus-containing culture medium were cultured in the medium containing 500 μg/ml G418 (Sigma Chemical Co., St. Louis, MO, USA). Two weeks after the selection in G418, drug-resistant clones were isolated and allowed to proliferate in medium containing G418.

## Reverse Transcription-PCR Analysis

Total RNA was prepared from cultured cells by using the RNeasy Mini Kit (Qiagen, Valencia, CA, USA). Reverse transcription was carried out using random primers and SuperScript II (Invitrogen). Following the reverse transcription, the resultant cDNA was subjected to PCR-based amplification. PCR primers used were as follows: human *LMO3*, forward 5′-ATGCTCTCAGTCCAGCCAGA-3′ and reverse 5′-TCAGCGAACCTGGGGTGCAT-3′; human *HEN2*, forward 5′-AAGCAGCAGATTCGGACCAT-3′ and reverse 5′-CTTCTCCTCGCGGCTCAG-3′; human *Mash1*, forward 5′-GCGTTCAGCACTGACTTTTG-3′ and reverse 5′-CCCCGGGAGACTTCTTAGAG-3′; human *HES1*, forward 5′-TGAGCCAGCTGAAAACACTG-3′ and reverse 5′-GTCACCTCGTTCATGCACTC-3; human *glyceraldehydes-3-phosphate dehydrogenase* (*GAPDH*), forward 5′-ACCTGACCTGCCGTCTAGAA-3′ and reverse 5′-TCCACCACCCTGTTGCTGTA-3′.

### RNA Interference Experiments

Human LMO3 RNAi vector was made using the original plasmid that is gift from A.K. Munirajan (Chiba Cancer Center Research Institute). The targeted sequence is 5′- GTAG-TAAGCTCATCCCTGC -3′. RNAi construct was transiently transfected into SH-SY5Y cells using Lipofectamine 2000 transfection reagent (Invitrogen, Carlsbad, CA, USA) according to the manufacturer's instruction.

### Generation of Recombinant Adenoviral Vector

For construction of the adenovirus expression vector, an HA-tagged human LMO3 cDNA or a FLAG-tagged human HEN2 cDNA were inserted into the shuttle vector pHMCMV6 [24]. Efficient construction of a recombinant adenovirus vector by an improved *in vitro* ligation method [25]. The resultant shuttle vector was digested with I-CeuI and PI-SceI and subcloned into the identical restriction sites of the adenovirus expression vector pAdHM4. The recombinant adenovirus construct was digested with *Pac*I and transfected into 293 cells to generate recombinant adenovirus.

### Luciferase Reporter Assay

The reporter plasmid contains a 1.2-kb fragment of the human *Mash1* promoter that was subcloned into the pGL3-Basic Vector (Promega Corp., Madison, WI, USA) upstream of the luciferase reporter gene. Cells were seeded in triplicates into 24-well plates ($1\times10^5$ cells/well) 24 h prior to transfection. Cells were cotransfected with 100 ng of the reporter plasmid, 0.2 ng of pRL-CMV encoding *Renilla* luciferase cDNA, 5 ng of rat HES1expression vector, 150 ng of HA-LMO3, 100 to 300 ng of FLAG-HEN2 expression vectors. Total amount of plasmid DNA per transfection was kept constant with pcDNA3 (Invitrogen). At 48 h after transfection, luciferase activity was measured by a Dual-Luciferase Reporter Assay System (Promega), and the transfection efficiency was standardized against *Renilla* luciferase activity.

### Chromatin Immunoprecipitation (ChIP) Assays

ChIP assay was performed according to the protocol recommended by Upstate (Lake Placid, NY, USA). Cross-linked chromatin prepared from Neuro2a cells transfected with expression plasmids was sonicated and immunoprecipitated with normal rabbit serum (NRS), polyclonal anti-Myc tag (Medical & Biological Laboratories, Nagoya, Japan) or with polyclonal anti-FLAG (Sigma, St. Louis, MO, USA) antibody. The genomic DNA was purified from the immunoprecipitates and amplified by PCR.

The primers used to amplify the mouse *Mash1* promoters were as follows: HES1 binding site (PCR-1), forward 5′-ATTTCTA-GAGCCACCCCCTG-3′ and reverse 5′-TTGTTGCAGTGCG-TGCGCC-3′; HES1 binding site (PCR-2), forward 5′-AGTGCGCTCGGCACTGACTT-3′ and reverse 5′-CGCG-GTTGGCTTCGGGAGCC-3′; E-box (PCR-3), forward 5′-ATGGAGAGTTTGCAAGGAGC-3′ and reverse 5′-CAGCCC-CACGCGCAGCCCTG-3′.

### Western Blot Analysis and Immunoprecipitation

After transfection, Neuro2a cells were placed on ice, washed twice with phosphate-buffered saline, and lysed in lysis buffer containing 25 mM Tris-HCl (pH 8.0), 137 mM NaCl, 2.7 mM KCl, 1% TritonX-100, 1 mM phenylmethylsulfonyl fluoride and protease inhibitor mixture (Sigma). Lysates were placed on ice for 30 min, sonicated briefly, and clarified by centrifugation at 15,000× *g* for 5 min at 4°C. Protein concentrations of the supernatants were determined by using a Bio-Rad protein assay. For immunoblot analysis, proteins were resolved by sodium dodecyl sulfatepolyacrylamide gel electrophoresis (SDS-PAGE) and electrotransferred onto a nitrocellulose membrane. The membrane filter was blocked with 2% gelatin in Tris-buffered saline (TBS) for 3 h at room temperature and then incubated with a primary antibody including monoclonal anti-rat HES1 (Medical & Biological Laboratories, Nagoya, Japan), monoclonal anti-FLAG (M2; Sigma) or monoclonal anti-Myc (9B11; Cell Signaling Technology, Danvers, MA, USA) antibody over night at 4°C. The membrane filter was then incubated with a goat anti-mouse secondary antibody conjugated to horseradish peroxidase (Cell Signaling Technology, Danvers, MA, USA) or goat anti-rat secondary antibody conjugated to horseradish peroxidase (Beckman Coulter, Marseille, France) for 1 h at room temperature and bound secondary antibody was detected by enhanced chemiluminescence (Amersham Pharmacia Biotech) according to the manufacturer's protocol. For Immunoprecipitation, equal amounts of cell lysates (2 mg) were precleared with 25 µl of protein G-Sepharose (Amersham Bioscience, Uppsala, Sweden). After brief centrifugation, immunoprecipitation was carried out by incubating the supernatant with anti-FLAG polyclonal (Sigma, St. Louis, MO, USA) or anti-Myc tag polyclonal antibody (Medical & Biological Laboratories, Nagoya, Japan) over night at 4°C. Immunocomplexes were precipitated with protein G-Sepharose beads (Amersham Biosciences) for 3 hours at 4°C. The immunoprecipitated proteins were resolved by SDS-PAGE and analyzed by Western blotting.

### *In vitro* Pull-down Assay

Radio-labeled FLAG-HEN2 was generated by using *in vitro* transcription/translation system (Promega) and incubated with cell lysates prepared from Neuro2a cells transfected with Myc-HES1 expression plasmid. The reaction mixture was immunoprecipitated with normal rabbit serum (NRS) or with polyclonal anti-Myc tag antibody (Medical & Biological Laboratories, Nagoya, Japan) and separated by SDS-PAGE followed by autoradiography.

### Data Analysis and Statistics

All values for statistical significance represent mean ± SD. We carried out comparisons between means using the Student's *t*-test. Statistical significance implies $P<0.05$.

## Supporting Information

**Figure S1 Mash1-mediated growth promotion and LMO3/HEN2-mediated transcriptional induction of *Mash1* in SK-N-BE cells.** (A) siRNA-mediated knockdown of LMO3. SK-N-BE cells were transfected with empty plasmid (4 µg) or with expression plasmid for siRNA targeting LMO3 (4 µg). Forty-eight hours after transfection, total RNA was prepared and analyzed for expression levels of *LMO3* and *Mash1* by RT-PCR. (B) Decreased growth rate in LMO3-knocked down cells. SK-N-BE cells ($4.5\times10^3$ cells/well, 96 well culture plate) were transfected with empty plasmid (0.2 µg) or with expression plasmid for siRNA targeting LMO3 (0.2 µg). Forty-eight hours after transfection, cells were transferred into fresh medium. At the indicated time points, cell growth was measured by MTT assay (Cell Counting Kit-8, DOJINDO). (C) RT-PCR. SK-N-BE cells were transfected with pcDNA3 empty plasmid or with the indicated combinations of expression plasmid HA-LMO3 or FLAG-HEN2. At 72 hours after transfection, total RNA was analyzed for expression levels of *LMO3*, *HEN2* and *Mash1* by RT-PCR. *GAPDH* was used as an internal control. (D) siRNA-mediated knockdown of LMO3 reduces the promoter activity of *Mash1*. SK-N-BE cells were co-

transfected with constant amount of pluc-Mash1 (100 ng) and pRL-CMV (0.2 ng) in the presence or absence of increasing amounts of expression plasmid for siRNA against human LMO3 (100 or 400 ng). Forty-eight hours after transfection, cells were lysed and their luciferase activities were measured.
(TIF)

**Figure S2 Expression of *LMO3*, *HEN2*, *Mash1* or *HES1* in neuroblastoma cell lines.** Semiquantitative RT-PCR analysis for expression of *LMO3*, *HEN3*, *Mash1* or *HES1* in neuroblastoma cell lines is performed under linear amplification conditions. Expression of *GAPDH* is shown as a control.
(TIF)

**Figure S3 Model for LMO3 and HEN2 cooperation in transcriptional regulation of *Mash1* in Neuroblastoma.** (A) HES1 binds to HES1 binding sites and E- box on *Mash1* promoter and represses *Mash1* transcription. (B) LMO3 inhibits recruitment of HES1 onto HES1-binding sites and E-box on *Mash1* promoter by forming complex with HES1, and thereby inducing the expression of Mash1. (C) HEN2 interferes with recruitment of HES1 onto HES1-binding sites and E-box on *Mash1* promoter by forming complex with HES1 and competing with HES1 in binding to these sites. HEN2 also represses *Mash1* transcription but the inhibitory effects are weaker than that of HES1, and so up-regulating transcription of *Mash1*. (D) LMO3 promotes recruitment of HEN2 onto HES1-binding sites and E-box on *Mash1* promoter by forming complex with HEN2 but inhibits negative effects of HEN2 on *Mash1* promoter. Furthermore, LMO3 inhibits recruitment of HES1 onto HES1-binding sites and E-box on *Mash1* promoter, and so *Mash1* may be more highly expressed.
(TIF)

**Table S1** Correlation between expression of LMO3 or Mash1 and other prognostic factors (Student's *t*-test).
(PDF)

**Table S2** Univariate and multivariate analyses of Mash1 and LMO3 mRNA expression as well as other prognostic factors in primary neuroblastomas.
(PDF)

## Acknowledgments

We are grateful to Dr. Ryuichiro Kageyama for providing the expression plasmid encoding HES1, to Drs. Nobutaka Hattori and Kaori Shiba for their valuable discussions. We also thank Yuki Nakamura for her technical assistance.

## Author Contributions

Conceived and designed the experiments: EI AN. Performed the experiments: EI. Analyzed the data: EI MO SO. Contributed reagents/materials/analysis tools: YN AN. Wrote the paper: EI MO TO AN.

## References

1. Nakagawara A (2004) Neural crest development and neuroblastoma: the genetic and biological link. In: Aloe L, Calzà L, eds: NGF and related molecules in health and disease, Progress in brain research. ELSEVIER. pp 14633–242.
2. Nakagawara A, Ohira M (2004) Comprehensive genomics linking between neural development and cancer: neuroblastoma as a model. Cancer Letters 204: 213–224.
3. Bach I (2000) The LIM domain: regulation by association. Mech Dev 91: 5–17.
4. Rabbitts TH (1998) LMO T-cell translocation oncogenes typify genes activated by chromosomal translocations that alter transcription and developmental processes. Genes Dev 12: 2651–2657.
5. Visvader JE, Venter D, Hahm K, Santamaria M, Sum EY, et al. (2001) The LIM domain gene LMO4 inhibits differentiation of mammary epithelial cells in vitro and is overexpressed in breast cancer. Proc Natl Acad Sci USA 98: 14452–14457.
6. Sum EY, Segara D, Duscio B, Bath ML, Field AS, et al. (2005) Overexpression of LMO4 induces mammary hyperplasia, promotes cell invasion, and is a predictor of poor outcome in breast cancer. Proc Natl Acad Sci USA 102: 7659–7664.
7. Aoyama M, Ozaki T, Inuzuka H, Tomotsune D, Hirato J, et al. (2005) LMO3 interacts with neuronal transcription factor, HEN2, and acts as an oncogene in neuroblastoma. Cancer Res 65: 4587–4597.
8. Gestblom C, Grynfeld A, Ora I, Ortoft E, Larsson C, et al. (1999) The basic helix-loop-helix transcription factor dHAND, a marker gene for the developing human sympathetic nervous system, is expressed in both high- and low-stage neuroblastomas. Lab Invest 79: 67–79.
9. Ichimiya S, Nimura Y, Seki N, Ozaki T, Nagase T, et al. (2001) Downregulation of hASH1 is associated with the retinoic acid-induced differentiation of human neuroblastoma cell lines. Med Pediatr Oncol 36: 132–134.
10. Kageyama R, Ohtsuka T, Kobayashi T (2007) The Hes family: repressors and oscillators that orchestrate embryogenesis. Development 134: 1243–1251.
11. Ramain P, Khechumian R, Khechumian K, Arbogast N, Ackermann C, et al. (2000) Interactions between chip and the achaete/scute-daughterless heterodimers are required for pannier-driven proneural patterning. Mol Cell 6: 781–790.
12. Asmar J, Biryukova I, Heitzler P (2008) *Drosophila* dLMO-PA isoform acts as an early activator of *achaete/scute* proneural expression. Developmental biology 316: 487–497.
13. Axelson H (2004) The Notch signaling cascade in neuroblastoma: role of the basic helix-loop-helix proteins HASH-1 and HES-1. Cancer Letters 204: 171–178.
14. Brown L, Baer R (1994) HEN1 encodes a 20-kilodalton phosphoprotein that binds an extended E-box motif as a homodimer. Mol Cell Biol 14: 1245–1255.
15. Wildner H, Gierl MS, Strehle M, Pla P, Birchmeier C (2008) Insm1 (IA-1) is a crucial component of the transcriptional network that controls differentiation of the sympatho-adrenal lineage. Development 135: 473–481.
16. Watt F, Watanabe R, Yang W, Agren N, Arvidsson Y, et al. (2007) A novel MASH1 enhancer with N-myc and CREB-binding sites is active in neuroblastoma. Cancer Gene Therapy 14: 287–296.
17. Bao J, Talmage DA, Role LW, Gautier J (2000) Regulation of neurogenesis by interactions between HEN1 and neuronal LMO proteins. Development 127: 425–435.
18. Bagley CG, Lipkowitz S, Gobel V, Mahon KA, Bertness V, et al. (1992) Molecular characterization of NSCL, a gene encoding a helix-loop-helix protein expressed in the developing nervous system. Proc Natl Acad Sci USA 89: 38–42.
19. Good DJ, Porter FD, Mahon KA, Parlow AF, Westphal H, et al. (1997) Hypogonadism and obesity in mice with a targeted deletion of the Nhlh2 gene. Nat Genet 15: 397–401.
20. Lanigan TM, DeRaad SK, Russo AF (1998) Requirement of the MASH-1 transcription factor for neuroendocrine differentiation of thyroid C cells. J Neurobiol 34: 126–134.
21. Tse E, Smith AJ, Hunt S, Lavenir I, Forster A, et al. (2004) Null mutation of the Lmo4 gene or a combined null mutation of the Lmo1/Lmo3 genes causes perinatal lethality, and Lmo4 controls neural tube development in mice. Mol Cell Biol 24: 2063–2073.
22. Brodeur GM (2003) Neuroblastoma: biological insights into a clinical enigma. Nat Rev Cancer 3: 203–216.
23. Morikawa Y, Zehir A, Maska E, Deng C, Schneider MD, et al. (2009) BMP signaling regulates sympathetic nervous system development through Smad 4-dependent and -independent pathways. Development 136: 3575–3584.
24. Mizuguchi H, Kay MA (1998) Efficient construction of a recombinant adenovirus vector by an improved *in vitro* ligation method. Hum Gene Ther 9: 2577–2583.
25. Mizuguchi H, Kay MA (1999) A simple method for constructing E1- and E1/E4-deleted recombinant adenoviral vectors. Hum Gene Ther 10: 2013–2017.

VOLUME 29 · NUMBER 24 · AUGUST 20 2011

JOURNAL OF CLINICAL ONCOLOGY

ORIGINAL REPORT

# Clinical and Biologic Features Predictive of Survival After Relapse of Neuroblastoma: A Report From the International Neuroblastoma Risk Group Project

*Wendy B. London, Victoria Castel, Tom Monclair, Peter F. Ambros, Andrew D.J. Pearson, Susan L. Cohn, Frank Berthold, Akira Nakagawara, Ruth L. Ladenstein, Tomoko Iehara, and Katherine K. Matthay*

Wendy B. London, Children's Oncology Group Statistics and Data Center and Dana-Farber Children's Hospital Cancer Center, Boston, MA; Victoria Castel, Unidad de Oncologia Pediatrica Hospital Universitario La Fe, Valencia, Spain; Tom Monclair, Oslo University Hospital, Oslo, Norway; Peter F. Ambros and Ruth L. Ladenstein, Children's Cancer Research Institute, St Anna Kinderkrebsforschung, Vienna, Austria; Andrew D.J. Pearson, Institute of Cancer Research and Royal Marsden Hospital, Surrey, United Kingdom; Susan L. Cohn, The University of Chicago, Chicago, IL; Frank Berthold, University Children's Hospital of Cologne, Germany; Akira Nakagawara, Chiba University, Chiba; Tomoko Iehara, Prefectural Medical University, Kyoto, Japan; and Katherine K. Matthay, University of California San Francisco School of Medicine, San Francisco, CA.

Submitted January 10, 2011; accepted May 26, 2011; published online ahead of print at www.jco.org on July 18, 2011.

Supported in part by the Little Heroes Pediatric Cancer Foundation and Forbeck Foundation (W.B.L.); by Grants No. FIS 09/02323 and GVBE10/08 from Generalitat Valenciana (V.C.); and by National Cancer Institute Grant No. PO1 81403, the Dougherty Foundation, the Conner Fund, and the Alex Lemonade Foundation (K.K.M.).

W.B.L. and V.C. contributed equally to this work.

Authors' disclosures of potential conflicts of interest and author contributions are found at the end of this article.

Corresponding author: Victoria Castel, Unidad de Oncologia Pediatrica, Hospital Universitario La Fe, 46009 Valencia, Spain; e-mail: castel_vic@gva.es.



0732-183X/11/2924-3286/$20.00

DOI: 10.1200/JCO.2010.34.3392

## ABSTRACT

### Purpose
Survival after neuroblastoma relapse is poor. Understanding the relationship between clinical and biologic features and outcome after relapse may help in selection of optimal therapy. Our aim was to determine which factors were significantly predictive of postrelapse overall survival (OS) in patients with recurrent neuroblastoma—particularly whether time from diagnosis to first relapse (TTFR) was a significant predictor of OS.

### Patients and Methods
Patients with first relapse/progression were identified in the International Neuroblastoma Risk Group (INRG) database. Time from study enrollment until first event and OS time starting from first event were calculated. Cox regression models were used to calculate the hazard ratio of increased death risk and perform survival tree regression. TTFR was tested in a multivariable Cox model with other factors.

### Results
In the INRG database (N = 8,800), 2,266 patients experienced first progression/relapse. Median time to relapse was 13.2 months (range, 1 day to 11.4 years). Five-year OS from time of first event was 20% (SE, ± 1%). TTFR was statistically significantly associated with OS time in a nonlinear relationship; patients with TTFR of 36 months or longer had the lowest risk of death, followed by patients who relapsed in the period of 0 to less than 6 months or 18 to 36 months. Patients who relapsed between 6 and 18 months after diagnosis had the highest risk of death. TTFR, age, International Neuroblastoma Staging System stage, and *MYCN* copy number status were independently predictive of postrelapse OS in multivariable analysis.

### Conclusion
Age, stage, *MYCN* status, and TTFR are significant prognostic factors for postrelapse survival and may help in the design of clinical trials evaluating novel agents.

*J Clin Oncol 29:3286-3292. © 2011 by American Society of Clinical Oncology*

## INTRODUCTION

Neuroblastoma is a genetically and clinically heterogeneous childhood malignancy arising from the embryonic sympathetic nervous system. Neuroblastoma is metastatic at diagnosis in approximately 50% of patients; more than half of children diagnosed with high-risk neuroblastoma will either not respond to conventional therapies or relapse after treatment, necessitating development of novel treatments. Little is known about how to identify patients who are more likely to respond to therapies and survive longer after primary treatment failure in such a heterogeneous disease. Selection of appropriate therapy is one way in which improved outcome can be achieved, so it is crucial to understand the clinical course of neuroblastoma after failure of conventional therapy.

The length of time from diagnosis to first relapse has been demonstrated to be of prognostic value in multiple types of pediatric tumors.[1-5] In one recent single-institution study of high-risk neuroblastoma, time to first relapse was shown to influence length of survival[6]; however, the relationship between initial tumor biologic and clinical risk factors was not extensively studied with regard to the length of second remission and survival after relapse. To gather additional information about the disease course after relapse, we queried the International Neuroblastoma Risk Group (INRG) database. The INRG project is a collaborative effort among cooperative pediatric oncology groups from Europe,

North America, Germany, Australia, New Zealand, and Japan. For the first time, we have a sufficiently large group of annotated relapsed or progressing patients with neuroblastoma to use to identify which clinical and biologic factors are most prognostic of postrelapse survival.[7] In this analysis of 2,266 patients with neuroblastoma who suffered relapse or progression, we show that time to first relapse is significantly associated with survival after relapse, in addition to several other biologic and clinical risk factors in multivariable analysis. This information may help guide therapeutic decisions and interpretation of clinical trials of novel agents.

## PATIENTS AND METHODS

### INRG Database

A total of 8,800 unique patients younger than 21 years of age with pathologically confirmed neuroblastoma who were diagnosed/enrolled between 1990 and 2002 comprise the INRG database.[7] An enrollment cutoff of 2002 was chosen to allow for sufficient follow-up time. Patients provided consent and were enrolled shortly after initial diagnosis onto one or more neuroblastoma clinical or biologic trials in Germany, Japan, Italy, Spain, or the United Kingdom or onto a North American Children's Oncology Group study or the European SIOP LNESG1 (International Society of Pediatric Oncology Localized Neuroblastoma European Study) trial. Institutional review board approval and informed patient consent were obtained by each country, cooperative group, and treating institution for their respective studies. In addition to date of diagnosis and follow-up data, information on 35 potential risk factors was included in the INRG database.[7] Of the 8,800 patients, the analytic cohort for this report is composed of 2,266 who experienced at least one event (relapse or progression of neuroblastoma or secondary malignancy) and who had available follow-up data. The only other analytic cohort inclusion requirement was that the first event was not death; patients who died at time of relapse/progression were excluded because their OS time could not be calculated. We are interested in patients who require a postrelapse treatment decision.

### Statistical Considerations

Time to first event was calculated as time from study enrollment to first occurrence of relapse, progression, or secondary malignancy or time of last patient contact if no event occurred. Overall survival (OS) time was calculated from first event until death or time of last contact if the patient was alive. For ease of discussion, throughout this article, we will refer to these concepts as time to first relapse (TTFR) and OS post relapse, respectively. The method of Kaplan-Meier was used to generate survival curves, and curves were compared using a two-sided log-rank test.[8] OS post relapse is presented as the 5-year point estimate (± SE; per method of Peto et al[9]).

The clinical and biologic factors at diagnosis analyzed are listed in Table 1.[7,10] For lactate dehydrogenase (LDH) and ferritin, median values from the entire INRG cohort (580 units/L and 96 ng/mL, respectively) were used to dichotomize patients as elevated or not elevated. We then chose to use data-driven splits in the risk to construct a survival tree rather than traditional predefined risk groups.

A Cox proportional hazards regression model was used to calculate the hazard ratio (HR) for increased risk of death (poor outcome category as compared with better outcome category).[11] Visual inspection of Kaplan-Meier curves and plots of log(-log(S(t))) versus log(t) were used to identify violations of the proportional hazards assumption.[12] Where the proportional hazards assumption was violated, Cox regression modeling was performed using time-dependent covariates to adjust for nonproportionality. Patients were categorized into 6-month cohorts (0 to $<6$, 6 to $<12$, 12 to $<18$, 18 to $<24$, 24 to $<30$, 30 to $<36$, and $\geq 36$ months) of TTFR for graphical presentation of the nonlinear relationship between TTFR and OS post relapse. Time-dependent covariates are somewhat analogous to the use of a squared term in an algebraic equation; to approximate the curve in Figure 2, we included a term for TTFR multiplied by OS time and a binary term for TTFR ($<365$ $v \geq 365$ days) in the Cox model. Inclusion of these terms in the model ensured that patients who progressed within a short time were weighted differently than those who relapsed after therapy.

Cox proportional hazards regression models were used to identify the most highly statistically significant variable to create a given split or branch in the survival tree,[11-14] and only the Table 1 variables that were statistically significant were tested in the survival tree. To account for the effect of TTFR, each step of the model included TTFR time-dependent covariates; these covariates were retained in all models regardless of their statistical significance. $P$ values less than .05 were considered statistically significant.[15]

## RESULTS

The clinical and biologic characteristics at diagnosis of the 2,266 relapsed/progressing patients are listed in Table 1. Seventy-three percent of patients were 18 months of age or older at diagnosis, 72% had stage 4 tumors, and 33% had *MYCN* amplified tumors. The median TTFR was 13.2 months (range, 1 day to 11.4 years), and for patients with *MYCN* amplified tumors (n = 562) or *MYCN* nonamplified tumors (n = 1,141), it was 11 months (range, 3 days to 7 years) and 14.5 months (range, 7 days to 11 years), respectively ($P < .001$).

### Univariate Survival Analyses

The 5-year OS post relapse was 20% (± SE, 1%; n = 2,266; Fig 1A). The median follow-up time of patients who did not die post relapse was 3.6 years (range, 1 day to 13.7 years). Most factors were statistically significantly associated with OS post relapse (Table 1), including unfavorable histology, stage 4, *MYCN* amplification, use of intensive multimodality treatment at diagnosis, age 547 days or older, elevated LDH, elevated ferritin, and high mitosis karyorrhexis index ($P < .001$; HR, $\geq 1.9$; Table 1).

TTFR was statistically significantly associated with OS time (Table 2), and a nonlinear relationship was identified (Fig 2). Traditional log-rank test comparisons of short versus long TTFR were not supported, because the required proportional hazards assumption was violated (eg, Fig 1B, using 365-day cutoff), regardless of the choice of the cutoff used to categorize patients as short versus long TTFR. TTFR had an effect on OS post relapse, but the strength of the effect varied for different lengths of TTFR (Fig 2). Each of the 6-month TTFR groups had a higher risk of death after relapse than patients with TTFR of 36 months or longer.

Patients at the highest risk of death were those who relapsed between 6 and 18 months after diagnosis (peak risk at approximately 12 months). Of patients who relapsed 12 months or longer after diagnosis, 24% underwent stem-cell transplantation during initial therapy, compared with only 10% who relapsed in less than 12 months. The risk of death is approximately the same (approximately 2.5 times higher than in patients with TTFR $\geq 36$ months) for patients who relapsed within 6 months as it was for patients who relapsed in 18 to less than 24 months. The group of children who relapsed within 6 months after diagnosis included an unexpectedly high proportion of patients with favorable risk factors. Of 461 children who relapsed within 6 months, 55% (255 of 461 patients) were younger than 18 months old at diagnosis in comparison with 20% (362 of 1,805 patients) of those who relapsed later than 6 months after diagnosis ($P < .001$; Appendix Table A1, online only). Similarly, 49% (219 of 448 patients) in the early relapse group had INSS stage 1, 2, 3, and 4S tumors, compared with only 23% of those (403 of 1,752 patients) who

**Table 1.** Clinical and Genetic Characteristics and Postrelapse Survival in the Relapsed INRG Cohort (n = 2,266)

| Factor | Patients | | Postrelapse OS | | 5-Year Postrelapse OS | Postrelapse OS *P*† |
|---|---|---|---|---|---|---|
| | No. | % | HR* | 95% CI | OS ± SE (%) | |
| Histologic classification‡ | | | 4.5 | 3.6 to 5.8 | | < .001 |
| Favorable | 246 | 27 | | | 66 ± 5 | |
| Unfavorable | 653 | 73 | | | 11 ± 2 | |
| INSS stage | | | 3.5 | 3.1 to 4.0 | | < .001 |
| 1, 2, 3, 4S | 622 | 28 | | | 52 ± 3 | |
| 4 | 1,578 | 72 | | | 8 ± 1 | |
| *MYCN* status | | | 2.7 | 2.4 to 3.1 | | < .001 |
| Nonamplified | 1,141 | 67 | | | 32 ± 2 | |
| Amplified | 562 | 33 | | | 7 ± 2 | |
| Initial treatment | | | 2.6 | 2.3 to 2.9 | | < .001 |
| Observation, surgery, or standard chemotherapy | 762 | 40 | | | 41 ± 3 | |
| Intensive multimodality | 1,143 | 60 | | | 7 ± 1 | |
| Age, days | | | 2.4 | 2.1 to 2.7 | | < .001 |
| < 547 | 617 | 27 | | | 47 ± 3 | |
| ≥ 547 | 1,649 | 73 | | | 10 ± 1 | |
| LDH, U/L | | | 2.4 | 2.1 to 2.8 | | < .001 |
| < 580 | 466 | 35 | | | 38 ± 2 | |
| ≥ 580 | 848 | 65 | | | 12 ± 2 | |
| Serum ferritin, ng/mL | | | 2.1 | 1.8 to 2.4 | | < .001 |
| < 96 | 321 | 28 | | | 34 ± 4 | |
| ≥ 96 | 839 | 72 | | | 12 ± 2 | |
| MKI‡ | | | 1.9 | 1.6 to 2.4 | | < .001 |
| Low, intermediate | 550 | 74 | | | 28 ± 3 | |
| High | 189 | 26 | | | 12 ± 4 | |
| 1p | | | 1.8 | 1.4 to 2.1 | | < .001 |
| No loss or aberration | 345 | 58 | | | 32 ± 5 | |
| LOH, deletion, or imbalance | 252 | 42 | | | 15 ± 3 | |
| Ploidy | | | 1.6 | 1.4 to 2.0 | | < .001 |
| > 1 (hyperdiploid) | 357 | 57 | | | 34 ± 4 | |
| ≤ 1 (diploid, hypodiploid) | 273 | 43 | | | 16 ± 4 | |
| Grade of NB differentiation‡ | | | 1.6 | 1.1 to 2.1 | | < .001 |
| Differentiating | 72 | 9 | | | 38 ± 8 | |
| Undifferentiated | 774 | 91 | | | 22 ± 3 | |
| Diagnostic category‡ | | | | | | |
| 1 (NB, stroma poor) | 992 | 91 | | | 21 ± 2 | |
| 2 (GNB, intermixed, stroma rich) | 5 | 0.5 | | | 0 | |
| 3 (GNB, well differentiated, stroma rich) | 5 | 0.5 | | | 0 | |
| 4 (GNB, nodular [composite]) | 90 | 8 | | | 10 ± 7 | |
| 2 and 3 *v* 1 and 4 | | | 1.4 | 0.8 to 2.4 | | .686 |
| 2 and 3 | 10 | 1 | | | 0 | |
| 1 and 4 | 1,082 | 99 | | | 20 ± 2 | |
| Year of diagnosis | | | 1.3 | 1.2 to 1.4 | | < .001 |
| ≥ 1996 | 1,333 | 59 | | | 25 ± 3 | |
| < 1996 | 933 | 41 | | | 17 ± 1 | |
| 11q | | | 1.1 | 0.8 to 1.5 | | .567 |
| Balanced or no aberration | 205 | 65 | | | 35 ± 6 | |
| Deletion, imbalance, or unbalanced | 115 | 35 | | | 20 ± 7 | |
| 17q | | | 1.1 | 0.7 to 1.6 | | .764 |
| No gain | 64 | 41 | | | 29 ± 8 | |
| Gain | 91 | 59 | | | 23 ± 9 | |

Abbreviations: GNB, ganglioneuroblastoma; HR, hazard ratio; INPC, International Neuroblastoma Pathology Classification; INRG, International Neuroblastoma Risk Group; INSS, International Neuroblastoma Staging System; LDH, lactate dehydrogenase; LOH, loss of heterozygosity; MKI, mitosis karyorrhexis index; NB, neuroblastoma; OS, overall survival.

*HRs denote increased risk of event for second row within given category as compared with first row.

†Per log-rank test.

‡Per INPC; per Shimada, if INPC missing.

  

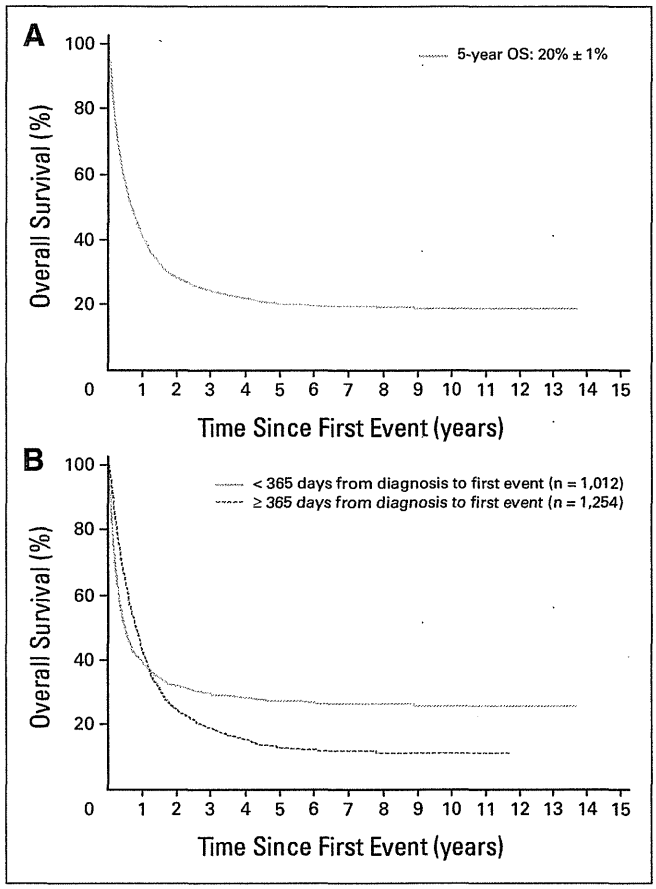


**Fig 1.** (A) Overall survival post relapse for 2,266 patients with neuroblastoma from the International Neuroblastoma Risk Group database. Median time to first relapse (TTFR) was 13.2 months (range, 1 day to 13.1 years). (B) Overall survival post relapse. TTFR less than 365 days from diagnosis (n = 1,012) versus TTFR 365 days or more from diagnosis (n = 1,254). Log-rank test *P* value is not valid because of violation of proportional hazards assumption, which can be seen in crossing of two curves.

relapsed later than 6 months ($P < .001$; Appendix Table A1, online only). Within the subset of relapsed patients who were stage 3 or 4 and *MYCN* amplified, the nonlinear relationship persisted (Fig 2), with a high risk of death for patients who relapsed within the first 12 months of diagnosis.

### *Multivariable Survival Analyses*

Although many factors were prognostic in a univariate test, few were prognostic in a multivariable Cox model (Table 3). Stage was the most highly predictive of OS post relapse, with increased risk of death for stages 4, 3, and 4S (6.9, 4.3, and 3.5 times higher than stages 1 and 2, respectively), with adjustment for TTFR by simultaneous inclusion in the Cox model.

The survival tree regression models identified a small proportion of patients who may have been salvageable after relapse (Fig 3). In the context of relapse therapy administered from 1990 to 2005, the salvageable cohorts seem to be those with stage 1, 2, 3, or 4S disease who had *MYCN* nonamplified tumors (excluding those with undifferentiated histology); those with stage 4 disease age younger than 18 months who had *MYCN* nonamplified tumors; and those with stage 1, 2, or 4S disease who had *MYCN* amplified tumors. Combined, approximately 15% of relapsed/progressing patients seemed to be curable. Within the survival tree subgroups, there were only two subgroups within which TTFR was statistically significantly associated with OS (ie, stage 4 patients with *MYCN* amplified tumors and stage 3 patients with *MYCN* amplified tumors).

## DISCUSSION

TTFR has been demonstrated to be prognostic in different pediatric tumors,[1-5] but it has not been thoroughly studied in neuroblastoma. Some studies have shown that a more chronic course of neuroblastoma after failure of primary therapy seems to be associated with longer times of first remission[16] or older age at diagnosis.[17-19] Cotterill et al[20] identified late relapse in a small subset of high-risk patients; however, this study was unable to predict which factors influence long-term survival given the limited follow-up.

In each of the single-institution studies, the number of patients and data collection were limited. In our analysis of 2,266 patients with relapsed neuroblastoma, we have shown that TTFR is an important factor to predict OS after an event. The relationship of TTFR and OS post relapse is complex; the risk of death was highest for patients who relapsed between 6 and 18 months from diagnosis and then decreased steadily, being lowest in patients who relapsed at 36 months or later. The association of TTFR and OS post relapse was the strongest in stage 3 and 4 patients with *MYCN* amplified tumors. Surprisingly, in the overall cohort, the risk of death for patients who relapsed between 6 and 18 months after diagnosis was higher than for patients who relapsed within 0 to 6 months, or more than 18 months, after diagnosis. A more intuitive relationship would be linear, where those with the shortest TTFR had the highest risk of death, with decreasing risk of death as TTFR increased. A possible explanation for why the patients with the shortest TTFR did not have the highest risk of death may lie in the more favorable clinical characteristics of the patients who relapsed within 6 months; a significantly larger proportion of patients were younger or had stage 1, 2, 3, or 4S disease in comparison with those who relapsed later. Patients who were younger and had a lower stage of disease may have received little or no therapy before relapse and therefore may have responded well to postrelapse treatment. Another possible explanation for the upward slope of the risk-of-death curve with TTFR of less than 12 months and the downward slope of the risk-of-death curve with TTFR of 12 months or longer (Fig 2) is that patients who are able to make it to transplantation (occurring approximately 10 to 12 months post diagnosis) without relapse/progression realize a benefit in terms of prolonged OS.

Accepted prognostic factors for neuroblastoma include age at diagnosis, *MYCN* gene amplification, and histologic features.[21] These factors are standard determinants of initial risk stratification, but their prognostic value after an event had not been studied previously. In our analysis, we identified several factors that were independently prognostic of OS after relapse: stage, *MYCN* status, age, and TTFR. Many other factors were significantly predictive of poor outcome after relapse in univariate, but not multivariable, analysis. Within the subgroups of patients with *MYCN* nonamplified tumors or stage 1, 2, or 4S disease, TTFR was not predictive of OS post relapse; it seems that the patients with INSS stage 3 and 4 *MYCN* amplified tumors were driving the association between TTFR and OS.

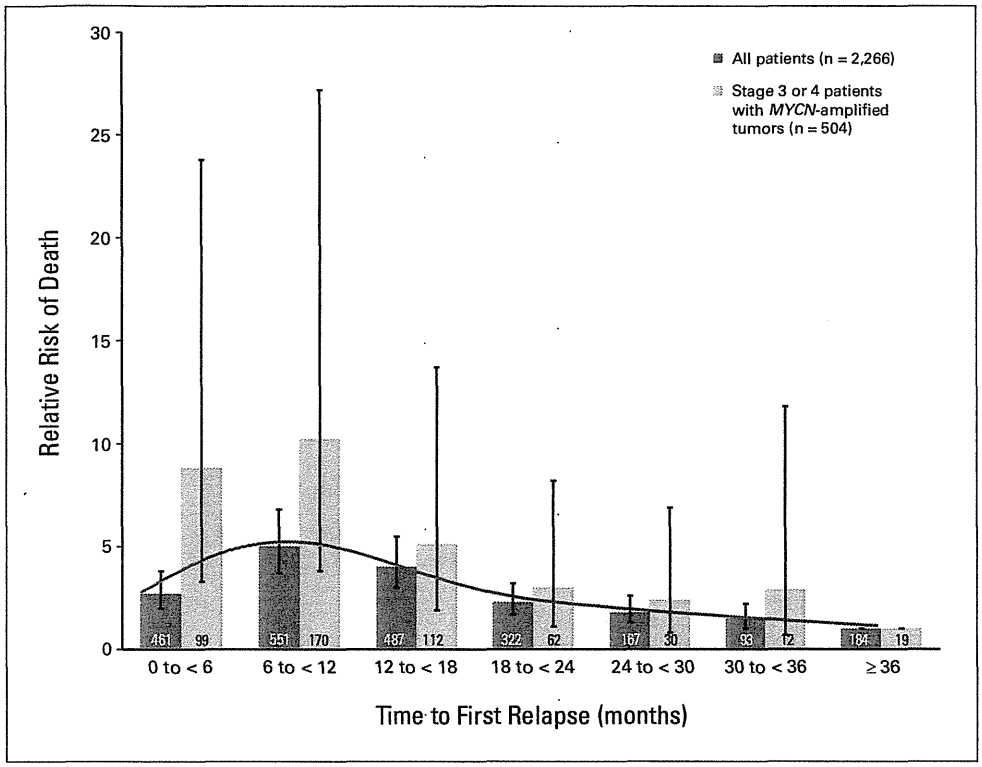


**Fig 2.** Relative risk (hazard ratio) of death for 6-month cohorts of time to first relapse in comparison with patients whose first relapse occurred more than 36 months from diagnosis. Patients whose first relapse occurred more than 36 months from diagnosis had a relative risk of death equal to 1. Blue bars are all patients (n = 2,266), and gold bars are the subset of stage 3 or 4 patients with *MYCN* amplified tumors (n = 504). SE bars are shown for relative risk of death for each cohort.

Two previous single-institution studies in neuroblastoma also showed that shorter time to first relapse was a significant adverse factor for survival.[6,16] Lau et al[16] reviewed 31 patients with neuroblastoma with relapsed disease and found that patients who relapsed less than 12 months from diagnosis had significantly shorter survival time. The only other significant factor in their analysis for survival post relapse was tumor *MYCN* amplification. Santana et al[6] addressed the study of disease-control intervals in 91 high-risk patients with neuroblastoma. The estimated median times to disease recurrence were 18.3, 8.7, and 3.8 months for the first, second, and third recurrences, respectively. Patients with longer initial disease control had a significant postrecurrence survival advantage. This study emphasized the importance of knowing the intervals of disease progression as end points for the design of protocols with new agents.[6]

Other studies in pediatric malignancies have also shown that earlier relapse portends shorter survival. The Italian Off-Therapy Registry published results on 694 patients, including those with neuroblastoma, CNS tumors, sarcoma, Wilm's tumors, and Hodgkin's lymphoma, who had experienced recurrence. They found significantly different HRs for survival by type of diagnosis and found overall that patients relapsing less than 12 months off therapy had worse survival in univariate, but not in multivariable, analysis.[22] Risk factors for survival post relapse in neuroblastoma

**Table 2.** Multivariable Analysis of OS After First Event.

| Time to First Relapse (months)* | No. of Patients | Risk of Death† | | |
|---|---|---|---|---|
| | | HR | 95% CI | *P* |
| 0 to < 6 | 461 | 2.7 | 2.0 to 3.8 | < .001 |
| 6 to < 12 | 551 | 5.0 | 3.7 to 6.8 | < .001 |
| 12 to < 18 | 487 | 4.0 | 3.0 to 5.5 | < .001 |
| 18 to < 24 | 322 | 2.3 | 1.7 to 3.2 | < .001 |
| 24 to < 30 | 167 | 1.8 | 1.3 to 2.6 | < .001 |
| 30 to < 36 | 93 | 1.5 | 1.0 to 2.2 | .063 |
| ≥ 36 | 184 | 1.0 | 1.0 to 1.0 | NA |

NOTE. Analysis testing of 6-month categories of time to first relapse compared with risk of death for those relapsing more than 36 months after diagnosis.

Abbreviations: HR, hazard ratio; NA, not applicable; OS, overall survival.

*All 6-month categories were simultaneously included in the model, except for ≥ 36, which was the reference level.

†In comparison with patients with first relapse more than 36 months after diagnosis.

**Table 3.** Clinical and Biologic Factors Independently Predictive of OS in Multivariable Analysis (n = 2,266)

| Variable* | Risk of Death | | |
|---|---|---|---|
| | HR | 95% CI | *P* |
| Stage 4 | 6.9 | 5.1 to 9.3 | < .001 |
| Stage 3 | 4.3 | 3.1 to 6.1 | < .001 |
| Stage 4S | 3.5 | 2.2 to 5.4 | < .001 |
| *MYCN* amplification | 2.4 | 2.1 to 2.7 | < .001 |
| Age ≥ 18 months | 1.6 | 1.4 to 1.9 | < .001 |
| TTFR < 12 months | 2.0 | 1.7 to 2.5 | < .001 |
| TTFR × OS time† | 1.0 | 1.0 to 1.0 | < .001 |

Abbreviations: HR, hazard ratio; OS, overall survival; TTFR, time to first relapse.

*Variables tested in multivariable model were those significant in survival tree regression: stage, *MYCN* status, age, ploidy, lactate dehydrogenase, and grade of differentiation.

†Interaction term consisting of 12-month TTFR cutoff multiplied by OS time is used to approximate curve shown in Figure 2.

  

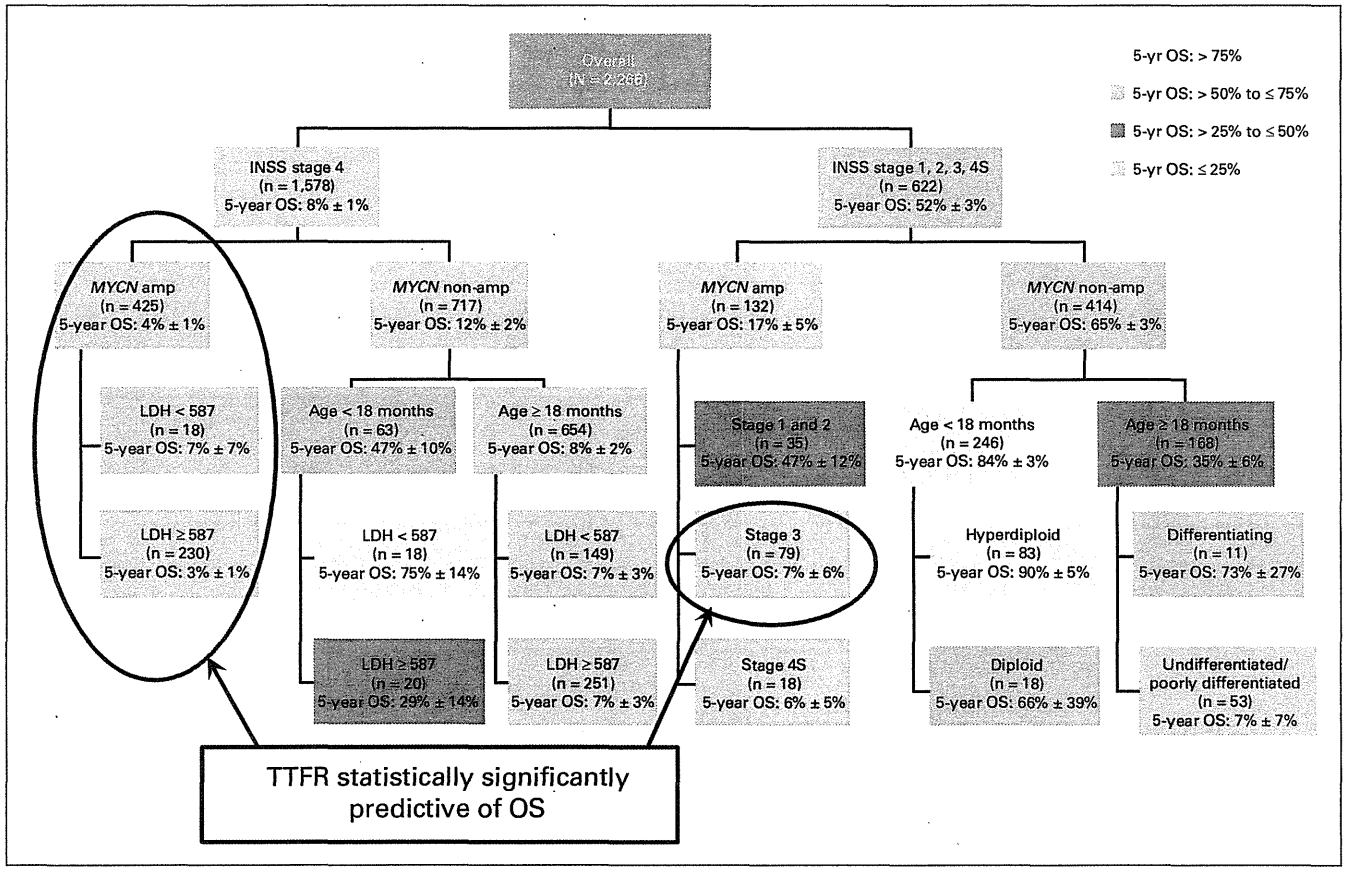


**Fig 3.** Survival tree regression of overall survival post relapse. Modeling was performed with adjustment for time to first relapse. Within each subgroup box, the value of OS post relapse is presented as the 5-year point estimate (± SE). INSS, International Neuroblastoma Staging System; LDH, lactate dehydrogenase; OS, overall survival; TTFR, time to first relapse.

were not evaluated separately. Interestingly, the patients relapsing in the more recent treatment era had shorter survival, perhaps because the relapse may have occurred after more intensive therapy. A similar trend has been reported in childhood leukemia, in which multiple studies have shown that duration of first remission was the most significant predictor of outcome after relapse of acute lymphoblastic leukemia.[4,5]

In a retrospective study, Garaventa et al[23] described 781 children with neuroblastoma experiencing tumor recurrence. Ten-year OS was 6.8% after progression and 14.4% after relapse. Similar to our series, the factors worsening prognosis in univariate analysis were age older than 18 months, advanced stage, high LDH, *MYCN* amplification, and abdominal primary (no multivariable analysis). Most relapses occurred early (median interval, 7.8 months), but 86 (24%) occurred late (median, 28 months). Early relapses had a more rapid, unfavorable course, with approximately 80% of deaths occurring within 2 years, whereas survival time was longer for late relapses.

From German protocols NB90, NB97, and NB2004 (n = 493 high-risk patients), Simon et al[24] presented data on 254 patients with neuroblastoma who relapsed after autologous bone marrow transplantation as part of initial treatment. *MYCN* amplification, early recurrence within 18 to 24 months after diagnosis, bone marrow, and lung/pleura metastasis at relapse were independently predictive of poor survival. The 24 patients who underwent a second autologous stem-cell transplantation had better outcome.

Ultimately, understanding the genetic differences in early versus late relapsing patients will facilitate selection of appropriate targeted therapy. Meanwhile, we propose that stratification of relapsed patients according to the timing of first relapse, as well as stage, age, and *MYCN* status, is critical in certain types of study designs, such as randomized phase II trials, to maintain a balance of less favorable patients between treatment arms. One might also wish to compare two strata for a given treatment to see which has better outcome. TTFR is a significant, readily available prognostic factor for stratification of patients on retrieval trials. In addition, TTFR may be used in therapy selection. Studies of novel agents using time to progression as an end point could be designed to stratify patients based on TTFR so that the effect of the novel agents can be separated from inherent tumor behavior.

We were not able to establish a single clear TTFR cutoff time point for stratification, perhaps because the INRG series is heterogeneous in relation to era of treatment and initial therapy received or because the true relationship between TTFR and OS post relapse is nonlinear. Our results demonstrate that the period from 6 to 18 months from diagnosis to relapse is associated with the shortest survival of relapsing patients, including the subset of patients with stage 3 and 4 *MYCN* amplified tumors.

In conclusion, time to first relapse is a significant predictor of death after relapse; the risk of death is higher for patients who relapse between 6 and 18 months after diagnosis than it is for patients who relapse more than 18 months from diagnosis. Stratification of relapsed patients with neuroblastoma according to the timing of first relapse,

age, stage, and *MYCN* status is important in retrieval study designs, especially for patients with stage 3 or 4 *MYCN* amplified tumors.

## AUTHORS' DISCLOSURES OF POTENTIAL CONFLICTS OF INTEREST

The author(s) indicated no potential conflicts of interest.

## AUTHOR CONTRIBUTIONS

**Conception and design:** Wendy B. London, Victoria Castel, Andrew D.J Pearson, Akira Nakagawara, Katherine K. Matthay

**Financial support:** Wendy B. London

**Administrative support:** Wendy B. London, Victoria Castel

**Provision of study materials or patients:** Victoria Castel, Peter F. Ambros, Frank Berthold, Akira Nakagawara, Ruth L. Ladenstein, Tomoko Iehara

**Collection and assembly of data:** Wendy B. London, Victoria Castel, Tom Monclair, Peter F. Ambros, Susan L. Cohn, Frank Berthold, Ruth L. Ladenstein, Tomoko Iehara

**Data analysis and interpretation:** Wendy B. London, Victoria Castel, Andrew D.J Pearson, Katherine K. Matthay

**Manuscript writing:** All authors

**Final approval of manuscript:** All authors

## REFERENCES


1. Barker LM, Pendergrass TW, Sanders JE, et al: Survival after recurrence of Ewing's sarcoma family of tumors. J Clin Oncol 23:4354-4362, 2005
2. Leavey P, Mascarenhas L, Marina N, et al: Prognostic factors for patients with Ewing sarcoma (EWS) at first recurrence following multi-modality therapy: A report from the Children's Oncology Group. Pediatr Blood Cancer 51:334-338, 2008
3. Dantonello T, Int-Veen C, Winkler P, et al: Initial patient characteristics can predict pattern and risk of relapse in localized rhabdomyosarcoma. J Clin Oncol 26:406-413, 2008
4. Malempati S, Gaynon P, Sather H, et al: Outcome after relapse among children with standard-risk acute lymphoblastic leukemia: Children's Oncology Group study CCG-1952. J Clin Oncol 25:5800-5807, 2007
5. Nguyen K, Devidas M, Cheng S, et al: Factors influencing survival after relapse from acute lymphoblastic leukemia: A Children's Oncology Group study. Leukemia 22:2142-2150, 2008
6. Santana V, Furman W, McGregor L, et al: Disease control intervals in high-risk neuroblastoma. Cancer 112:2796-2801, 2008
7. Cohn S, Pearson A, London W, et al: The International Neuroblastoma Risk Group (INRG) classification system: An INRG Task Force report. J Clin Oncol 27:289-297, 2009
8. Kaplan EL, Meier P: Nonparametric estimation from incomplete observations. J Am Stat Assoc 53: 457-481, 1958
9. Peto R, Pike M, Armitage P, et al: Design and analysis of randomized clinical trials requiring prolonged observation of each patient: I. Introduction and design. Br J Cancer 34:585-612, 1976
10. Ambros PF, Ambros IM, Brodeur GM, et al: International consensus for neuroblastoma molecular diagnostics: Report from the International Neuroblastoma Risk Group (INRG) Biology Committee. Br J Cancer 100:1471-1482, 2009
11. Cox DR: Regression models and life-tables. J R Stat Soc 34:187-220, 1972
12. Segal MR: Regression trees for censored data. Biometrics 44:35-47, 1988
13. Davis RB, Anderson JR: Exponential survival trees. Stat Med 8:947-961, 1989
14. Leblanc M, Crowley J: Survival trees by goodness of split. J Am Stat Assoc 88:457-467, 1993
15. Fleming TR, Harrington DP: Counting Processes and Survival Analysis. New York, NY, John Wiley & Sons, 1991
16. Lau L, Tai D, Weitzman S, et al: Factors influencing survival in children with recurrent neuroblastoma. J Pediatr Hematol Oncol 26:227-232, 2004
17. Kushner BH, Kramer K, Cheung NK: Chronic neuroblastoma. Cancer 95:1366-1375, 2002
18. Franks LM, Bollen A, Seeger RC, et al: Neuroblastoma in adults and adolescents: An indolent course with poor survival. Cancer 79:2028-2035, 1997
19. Conte M, Parodi S, De Bernardi B, et al: Neuroblastoma in adolescents: The Italian experience. Cancer 106:1409-2006;
20. Cotterill SJ, Pearson AD, Pritchard J, et al: Late relapse and prognosis for neuroblastoma patients surviving 5 years or more: A report from the European Neuroblastoma Study Group "Survey." Med Pediatr Oncol 36:235-238, 2001
21. George RE, Variend S, Cullinane C, et al: Relationship between histopathological features, MYCN amplification, and prognosis: A UKCCSG study United Kingdom Children Cancer Study Group. Med Pediatr Oncol 36:169-176, 2001
22. Ceschel S, Casotto V, Valsecchi M, et al: Survival after relapse in children with solid tumors: A follow-up study from the Italian off-therapy registry. Pediatr Blood Cancer 47:560-566, 2006
23. Garaventa A, Parodi S, De Bernardi B, et al: Outcome of children with neuroblastoma after progression or relapse: A retrospective study of the Italian neuroblastoma registry. Eur J Cancer 45:2835-2842, 2009
24. Simon T, Berthold F, Klingenbiel T, et al: Do relapsed high risk neuroblastoma patients have a second chance? Pediatr Blood Cancer 53; 5:736, 2009


  

Published OnlineFirst September 9, 2011; DOI:10.1158/1078-0432.CCR-11-0313

Clinical Cancer Research

# Expression of *NLRR3* Orphan Receptor Gene Is Negatively Regulated by MYCN and Miz-1, and Its Downregulation Is Associated with Unfavorable Outcome in Neuroblastoma

Jesmin Akter, Atsushi Takatori, Md. Shamim Hossain, et al.

*Clin Cancer Res* 2011;17:6681-6692. Published OnlineFirst September 9, 2011.

Published OnlineFirst September 9, 2011; DOI:10.1158/1078-0432.CCR-11-0313

Human Cancer Biology

Clinical Cancer Research

# Expression of *NLRR3* Orphan Receptor Gene Is Negatively Regulated by MYCN and Miz-1, and Its Downregulation Is Associated with Unfavorable Outcome in Neuroblastoma

Jesmin Akter[1,2], Atsushi Takatori[1], Md. Shamim Hossain[1], Toshinori Ozaki[1,3], Atsuko Nakazawa[5], Miki Ohira[4], Yusuke Suenaga[1], and Akira Nakagawara[1,2]

## Abstract

**Purpose:** Our previous study showed that expression of NLRR3 is significantly high in favorable neuroblastomas (NBL), whereas that of NLRR1 is significantly high in unfavorable NBLs. However, the molecular mechanism of transcriptional regulation of *NLRR3* remains elusive. This study was undertaken to clarify the transcriptional regulation of *NLRR3* and its association with the prognosis of NBL.

**Experimental Design:** *NLRR3* and *MYCN* expressions in NBL cell lines were analyzed after induction of cell differentiation, MYCN knockdown, and overexpression. The transcriptional regulation of *NLRR3* was analyzed by luciferase reporter and chromatin immunoprecipitation assays. Quantitative PCR was used for examining the expression of *NLRR3*, *Miz-1*, or *MYCN* in 87 primary NBLs.

**Results:** The expression of *NLRR3* mRNA was upregulated during differentiation of NBL cells induced by retinoic acid, accompanied with reduced expression of *MYCN*, suggesting that *NLRR3* expression was inversely correlated with *MYCN* in differentiation. Indeed, knockdown of *MYCN* induced *NLRR3* expression, whereas exogenously expressed MYCN reduced cellular *NLRR3* expression. We found that Miz-1 was highly expressed in favorable NBLs and *NLRR3* was induced by *Miz-1* expression in NBL cells. MYCN and Miz-1 complexes bound to *NLRR3* promoter and showed a negative regulation of *NLRR3* expression. In addition, a combination of low expression of *NLRR3* and high expression of *MYCN* was highly associated with poor prognosis.

**Conclusions:** *NLRR3* is a direct target of MYCN, which associates with Miz-1 and negatively regulates *NLRR3* expression. NLRR3 may play a role in NBL differentiation and the survival of NBL patients by inversely correlating with *MYCN* amplification. *Clin Cancer Res; 17(21); 6681–92. ©2011 AACR.*

## Introduction

Neuroblastoma (NBL) is one of the most common malignant solid tumors in children and accounts for 8% of all pediatric cancers (1). NBLs originate from sympathetic precursor neuroblasts derived from the neural crest. NBLs found in patients older than 1 year are usually aggressive and eventually kill the patients despite intensive therapy, whereas those in patients younger than 1 year often regress spontaneously or maturate, resulting in a favorable prognosis (2). We have made extensive efforts to show that TrkA, a high-affinity receptor for nerve growth factor, and TrkB, a receptor for brain-derived neurotrophic factor as well as neurotrophin 4/5, are important key regulators (3–6). However, the precise molecular mechanisms of how NBL becomes aggressive and how the spontaneous regression is induced still remain elusive.

Amplification of the *MYCN* oncogene is strongly associated with rapid progression of NBL (7). The *MYCN* amplification occurs in approximately 25% of NBL and is one of the most important prognostic indicators of poor clinical outcome (8–12). MYCN is a nuclear transcription factor and its expression level is well associated with cell proliferation of NBL cells (13, 14). In general, MYCN exerts its biological functions through transcriptional regulation of its target genes in both positive and negative manners. MYCN has an ability to activate its target genes by forming a heterodimer with MAX and binds to the E-box motif, CACGTG, in the proximal promoter region (15–18). On the contrary, MYCN represses the expression of genes, such

**Authors' Affiliations:** [1]Division of Biochemistry and Innovative Cancer Therapeutics, Chiba Cancer Center; [2]Department of Molecular Biology and Oncology, Chiba University Graduate School of Medicine; [3]Laboratories of Anti-Tumor Research and [4]Cancer Genomics, Chiba Cancer Center Research Institute, Chiba; and [5]Department of Pathology, National Center for Child Health and Development, Tokyo, Japan

**Note:** Supplementary data for this article are available at Clinical Cancer Research Online (http://clincancerres.aacrjournals.org/).

**Corresponding Author:** Akira Nakagawara, Division of Biochemistry and Innovative Cancer Therapeutics, Chiba Cancer Center, 666-2 Nitona, Chuoh-ku, Chiba 260-8717, Japan. Phone: 81-43-264-5431; Fax: 81-43-265-4459; E-mail: akiranak@chiba-cc.jp

**doi:** 10.1158/1078-0432.CCR-11-0313

Published OnlineFirst September 9, 2011; DOI:10.1158/1078-0432.CCR-11-0313



**Translational Relevance**

Amplification of *MYCN* oncogene is strongly associated with rapid progression of neuroblastoma (NBL) and one of the most important prognostic indicators of poor clinical outcome. Our group previously reported that NLRR3 is highly expressed in a favorable subset of NBL but until this work, there was no sound investigation of the function of NLRR3 and its transcriptional regulation. In this study, we found that *NLRR3* is a direct target of MYCN but its expression is negatively regulated by MYCN in association with Miz-1. Furthermore, a combination of low expression level of *NLRR3* and high expression level of *MYCN* was strongly correlated with the poor prognosis. These data suggest that the expression pattern of NLRR3, Miz-1, and MYCN plays an important role in defining the clinical behavior of NBLs. The decreased expression of NLRR3 might be one of the key events regulating the aggressive behavior of NBL.

as $p15^{INK4b}$, $p21^{CIP1}$, and *NDRG2*, when it forms a complex with transcriptional regulators, such as Myc-interacting zinc finger protein 1 (Miz-1) and Sp1 (19–21). Koppen and colleagues have previously described that MYCN suppresses *Dickkopf-1* (*DKK1*) expression, resulting in proliferation of NBL cells (22). However, the precise mechanism of how MYCN contributes to NBL aggressiveness remains unclear.

We have identified human neuronal leucine-rich repeat (NLRR) family genes as one of the differentially expressed genes between favorable and unfavorable NBLs, using our unique NBL cDNA libraries (23, 24). The NLRR protein family consists of 3 members, NLRR1, NLRR2, and NLRR3 (23), and belongs to the type *y* transmembrane protein with leucine-rich repeat (LRR) domains containing 11 or 12 LRRs, an immunoglobulin c2-type domain, and a fibronectin type III domain in its extracellular region. The amino acid sequences of NLRR family proteins are highly conserved in the extracellular domains, and NLRR1 and NLRR3 also possess a conserved stretch of 11 amino acids with 2 clathrin adapter interaction domains and a dileucine-type domain in the short intracellular region (25, 26), which might provide a basis for NLRR function. Our previous reports showed that NLRR1 is a direct transcriptional target of MYCN and that a high expression level of *NLRR1* mRNA is associated with a poor prognosis of NBL (23, 27). However, the function of NLRR3 is poorly understood except that mouse *NLRR3* expression is increased in the cerebral cortex after a cortical brain injury (28) and that rat NLRR3 may be involved in the regulation of EGF receptor signaling through interaction with clathrins (26).

We have previously reported that high levels of *NLRR3* mRNA expression are associated with favorable prognostic factors in NBL (23). In this study, we found that NLRR3 is induced during differentiation of NBL cells. Transcriptional analysis has revealed that NLRR3 is a direct transcriptional target of MYCN, which negatively transactivates it in association with Miz-1. Furthermore, high expression of *NLRR3* or *Miz-1* and the combination of high expression of both *NLRR3* and *Miz-1* are significantly associated with a favorable outcome of NBL. On the contrary, the low expression levels of *NLRR3* and high expression of *MYCN* were strongly correlated with a poor prognosis of NBL.

## Materials and Methods

### Patient population

Eighty-seven patients with NBL were diagnosed clinically and histologically, using a surgically removed tumor specimen according to the International Neuroblastoma Pathological classification (INPC). According to the International NBL Staging System (INSS; ref. 29), 18 patients were diagnosed as stage 1, 11 were stage 2, 20 were stage 3, 33 were stage 4, and 5 were stage 4S. Cytogenetic and molecular biological analysis of all tumors was also carried out by assessing DNA ploidy, *MYCN* amplification, and *TrkA* expression. The patients were then treated following the protocols proposed by the Japanese Infantile NBL Cooperative Study (30) and Group for Treatment of Advanced NBL (31), and subjected to survival analysis of the result in a follow-up period of at least 36 months (range, 4–58). The study was conducted under internal review board approval with appropriate informed consent.

### Cell lines and transient transfection

Human NBL-derived cell lines, including SK-N-BE, CHP134, IMR32, GOTO, KAN, KP-N-NS, LAN-5, NB-1, NB-9, NLF, RTBM1, SK-N-DZ, TGW, NB69, NBL-S, OAN, SK-N-AS, SK-N-SH, and SH-SY5Y cells were obtained from the CHOP cell line bank (Philadelphia, PA) and maintained in a culture condition, using RPMI 1640 supplemented with 10% heat-inactivated FBS (Invitrogen), 100 IU/mL penicillin, and 100 μg/mL streptomycin in a 37°C, 5% $CO_2$ incubator. For the NBL cell differentiation experiment, RTBM1 and SH-SY5Y cells were exposed to all-*trans* retinoic acid (ATRA; Sigma) at a final concentration of 5 μmol/L. For transient transfection, cells were transfected with the indicated expression of plasmids by using a Lipofectamine 2000 transfection reagent (Invitrogen), according to the manufacturer's recommendations.

### RNA extraction and semiquantitative reverse transcriptase PCR

Total RNA was prepared from fresh-frozen tissues of primary NBLs or cultured cells by using Trizol reagents (Life Technologies) or the RNeasy Mini kit (Qiagen). Reverse transcription was carried out by random primers and Superscript II (Invitrogen), following the manufacturer's instructions. After reverse transcription, the resultant cDNA was subjected to PCR-based amplification. The sequence of the primer sets were used for PCR amplification is listed in the Supplementary Table S4. All PCR amplifications were carried out with a GeneAmp PCR 9700 (Perkin-Elmer Co), using rTaq DNA polymerase (Takara).

Published OnlineFirst September 9, 2011; DOI:10.1158/1078-0432.CCR-11-0313



The expression of *GAPDH* was measured as an internal control.

**Quantitative real-time PCR**

cDNA from primary NBLs and cell lines were subjected to the real-time PCR to quantitate the expression levels of *MYCN*, *Miz-1*, and *NLRR3* mRNA. TaqMan GAPDH control reagent kit (Perkin-Elmer Applied Biosystems) was used for *GAPDH* expression and analyzed by an ABI prism 7500 Sequence Detection System (Applied Biosystems). *NLRR3* and *Miz-1* TaqMan probes were purchased from Applied Biosystems. *MYCN* mRNA expression was measured by the SYBR green real-time PCR system. The primers and probes used for real-time PCR were listed in Supplementary Table S4.

**Generation of a specific antibody against NLRR3**

The rabbit polyclonal anti-NLRR3 antibody was raised against a mixed synthetic peptide corresponding to amino acid sequences between positions 655 to 670 and 692 to 707 of human NLRR3. The peptide and polyclonal antibody (TB0266) were generated by Medical and Biological Laboratories (Nagoya, Japan). The specificity of the affinity-purified antibody was assayed by immunoblotting.

**Plasmid constructs**

The protein-coding region of *Miz-1* was amplified by PCR and inserted into the *Eco*RI site of pcDNA3.1 (Invitrogen) flanked with a Flag tag. The human *NLRR3* promoter region and its 5′ progressive deletion mutant were amplified by PCR and then inserted into the *Sacy* site in the upstream of the luciferase gene of the pGL3-basic plasmid (Promega). All constructs were verified by DNA sequencing. The pUHD-MYCN vector was kindly provided by Dr. M. Schwab (German Cancer Research Center, Heidelberg, Germany).

**Luciferase reporter assay**

SH-SY5Y cells were seeded at a density of $5 \times 10^4$ cells/12-well cell culture plate and allowed to attach overnight. The cells were transiently cotransfected with each mutant of the human *NLRR3* promoter-driven luciferase reporter and an internal control vector for *Renilla* luciferase, or a combination of the indicated expression vectors. The total amount of plasmid DNA per transfection was kept consistent with the pcDNA3.1 vector. Both firefly and *Renilla* luciferase activities were assayed with the Dual-Luciferase reporter assay system (Promega) according to the manufacturer's instructions. The firefly luminescence signal was normalized on the basis of the *Renilla* luminescence signal.

**siRNA transfection**

To knockdown endogenous MYCN expression, SK-N-AS, SK-N-BE, and SH-SY5Y cells were transfected with 10 nmol/L of the indicated siRNA purchased from Dharmacon by using LipofectAMINE RNAiMAX (Invitrogen), according to the manufacturer's recommendations. The list of siRNA sequences used will be provided upon request. Forty-eight hours after transfection, cell lysates were prepared and analyzed for the expression levels of NLRR3 and MYCN by immunoblotting.

**Immunoblot analysis**

The cells were washed twice with ice-cold PBS and then lysed immediately with SDS sample buffer containing 10% glycerol, 5% β-mercaptoethanol, 2.3% SDS, and 62.5 mmol/L Tris-HCl (pH 6.8). The protein concentrations were determined by using Bio-Rad protein assay dye reagent (Bio-Rad Laboratories). Equal amounts of cell lysates were separated by SDS-PAGE and electrophoretically transferred onto Immobilon-P membranes (Millipore). The transferred membranes were blocked with 5% nonfat dry milk in TBS containing 0.1% Tween-20 and incubated with appropriate primary antibodies at room temperature for 1 hour followed by incubation with horseradish peroxidase–conjugated goat anti-mouse or anti-rabbit secondary antibodies (Cell Signaling Technology Inc.) at room temperature for 1 hour. Immunoreactive bands were visualized by an ECL system (GE Healthcare). The primary antibodies used in this study were as follows: monoclonal anti-MYCN (Ab-1; Oncogene Research Products), polyclonal anti-NLRR3, polyclonal anti–Miz-1 (Santa Cruz Biotechnology), monoclonal anti-GAP43 (9-1E21; Chemicon), and polyclonal anti-actin (20-33; Sigma) antibodies.

**Chromatin immunoprecipitation assays**

A chromatin immunoprecipitation (ChIP) assay was carried out according to the protocol provided by Upstate Biotechnology (Charlottesville). In brief, cells were cross-linked with 1% formaldehyde in medium for 10 minutes at 37°C. Chromatin solutions were prepared and immunoprecipitated with the following antibodies: anti-MYCN, anti–Miz-1, anti-Max rabbit polyclonal antibodies (Santa Cruz Biotechnology), and normal mouse or rabbit serum as a control. The immunoprecipitates were eluted with 100 μL of elution buffer (1% SDS and 1 mmol/L $NaHCO_3$). Formaldehyde-mediated cross-links were reversed by heating at 65°C for 4 hours, and the reaction mixtures were treated with proteinase K at 45°C for 1 hour. DNAs of the immunoprecipitates and control input DNAs were purified by using a QIAquick PCR purification kit (Qiagen). Purified DNA was subjected to optimized semiquantitative PCR amplification protocol for NLRR3 gene promoter and control regions, using appropriate primer sets (Supplementary Table S4).

**Statistical analysis**

Student *t* tests were employed to examine the possible association between *NLRR3* expression and other prognostic factors. The classification of high and low levels of *NLRR3*, *Miz-1*, and *MYCN* expression was determined on the basis of the mean value obtained from quantitative real-time PCR analysis. Kaplan–Meier survival curves were calculated, and survival distributions were compared by using the log-rank test. Cox regression models were used to search associations along with *NLRR3* expression, *MYCN*

Published OnlineFirst September 9, 2011; DOI:10.1158/1078-0432.CCR-11-0313



expression, *Miz-1* expression, age, *MYCN* amplification status, INSS, *TrkA* expression, DNA index, origin, and survival. Statistical significance was considered if *P* value was less than 0.05. The statistical analysis was carried out by SPSS Statistical Software release 12.0.

## Results

### *NLRR3* is upregulated during neuronal differentiation

It has been previously reported that the NBL cell lines exposed to ATRA undergo neuronal differentiation (32), accompanied by a marked decrease in the expression levels of *MYCN* (33). To examine the possible involvement of MYCN in the regulation of NLRR3 expression, the NBL-derived RTBM1 cells were treated with or without 5 μmol/L ATRA. As previously described (34), RTBM1 cells underwent neuronal differentiation with extensive neurite outgrowth in response to ATRA treatment (Fig. 1A). The induced differentiation was confirmed by the expression levels of *GAP43*, a marker of neuronal differentiation (35), which increased after ATRA treatment at both mRNA and protein levels (Fig. 1B and C). As expected, MYCN expression was significantly decreased after ATRA treatment and almost diminished at 6 days after treatment. Consistent with our previous observations (23), *NLRR3* was markedly upregulated at the mRNA and protein levels during the differentiation process. Similar results were also obtained from ATRA-treated SH-SY5Y cells (Supplementary Fig. S1A and B).

### Inverse correlation between *MYCN* and *NLRR3* expressions

To further confirm a possible relationship between MYCN and NLRR3, we used MYCN-inducible SHEP21N cells originally derived from NBL (36) and treated with tetracycline to switch off the expression of MYCN. As shown in Fig. 2A, the reduced expression level of *MYCN* upon tetracycline treatment was confirmed by reverse transcriptase PCR (RT-PCR) and immunoblotting, whereas NLRR3 expression was increased after tetracycline treatment.

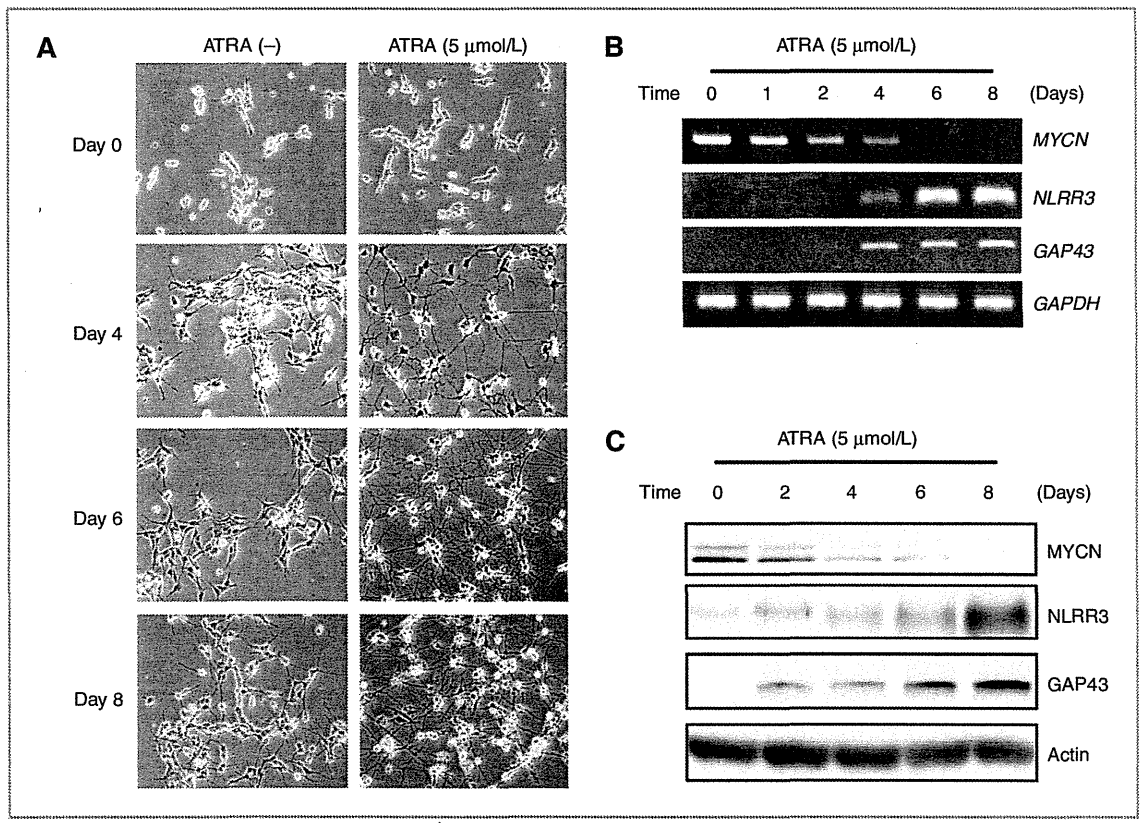


Figure 1. Opposite expression pattern of *NLRR3* and *MYCN* in differentiated RTBM1 cells in response to ATRA. A, ATRA-induced differentiation program in RTBM1 cells. Cells were treated with 5 μmol/L ATRA or left untreated. At the indicated time-periods after treatment with ATRA, neurite outgrowth was examined with a phase-contrast microscope. B and C, RT-PCR and immunoblot analysis for MYCN, NLRR3, and GAP43 in response to ATRA. RTBM1 cells were treated as in A. Total RNA and cell lysates were prepared and processed for RT-PCR (B) and immunoblotting with indicated antibodies (C). For RT-PCR, *GAPDH* was used as an internal control. For immunoblotting, actin was used as a loading control.

Published OnlineFirst September 9, 2011; DOI:10.1158/1078-0432.CCR-11-0313



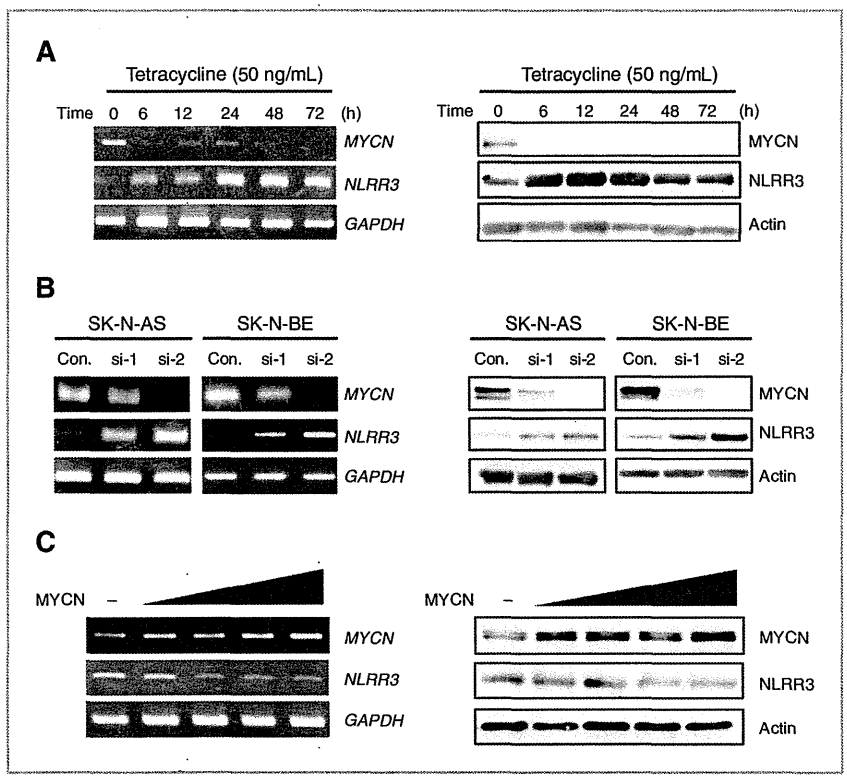


Figure 2. Inverse regulation of MYCN and NLRR3 in various NBL cell lines. A, RT-PCR and immunoblot analysis for MYCN and NLRR3 in SHEP21N cells maintained in the presence of tetracycline. At the indicated time points after the addition of tetracycline (50 ng/mL), total RNA and cell lysates were prepared and processed for RT-PCR (left) and immunoblotting with indicated antibodies (right). B, siRNA-mediated knockdown of the endogenous MYCN. SK-N-AS and SK-N-BE cells were transfected with control siRNA (Con.) or with 2 siRNA (si-1 and si-2) against MYCN. At 48 hours after transfection, total RNA and cell lysates were prepared and processed for RT-PCR (left) and immunoblotting with indicated antibodies (right). C, SH-SY5Y cells were transiently transfected with or without the increasing amounts of the expression plasmid encoding MYCN. Forty-eight hours after transfection, total RNA and cell lysates were prepared and processed for RT-PCR (left) and immunoblotting (right) with indicated antibodies. *GAPDH* was used as an internal control of RT-PCR and actin was used as a loading control for immunoblotting.

To examine whether MYCN and NLRR3 have an inverse functional relationship under these physiologic conditions, siRNA knockdown of the endogenous MYCN was carried out in 2 NBL cell lines, SK-N-AS cells with a single copy of *MYCN* and SK-N-BE cells with *MYCN* amplification. As shown in Fig. 2B, one of the siRNAs against *MYCN*, si-2, efficiently reduced endogenous expression of *MYCN* in both cell lines and resulted in an increased expression of NLRR3. SH-SY5Y cells with a single copy of *MYCN* also showed the similar result after siRNA-mediated knockdown of the endogenous MYCN (Supplementary Fig. S2A and B). These observations prompted us to examine whether MYCN can directly downregulate *NLRR3* expression. To address this issue, SH-SY5Y NBL cells were transfected with the expression plasmid encoding the *MYCN* gene. Forced expression of MYCN resulted in a dose-dependent decrease of NLRR3 expression both at the mRNA and protein levels (Fig. 2C), suggesting that *NLRR3* expression is negatively regulated by MYCN in NBL cells.

### MYCN represses the promoter activity of *NLRR3* in association with Miz-1

According to the previous reports (19, 20, 37), Myc proteins repress its target genes by forming a complex with Miz-1. Under these conditions at low expression levels of Myc, Miz-1 activates transcription of the target genes by cooperating with other transcriptional cofactors and enhances cell differentiation (20). Therefore, we hypothesized that Miz-1 might be involved in the regulation of *NLRR3* expression. To prove this, we examined whether exogenously expressed Miz-1 upregulates *NLRR3* expression in SH-SY5Y cells. Figure 3A, left shows that *NLRR3* expression was upregulated by overexpression of Miz-1 in the same manner as a positive control, $p15^{Ink4b}$ expression, whereas expression of other NLRR family members, *NLRR1*

Published OnlineFirst September 9, 2011; DOI:10.1158/1078-0432.CCR-11-0313



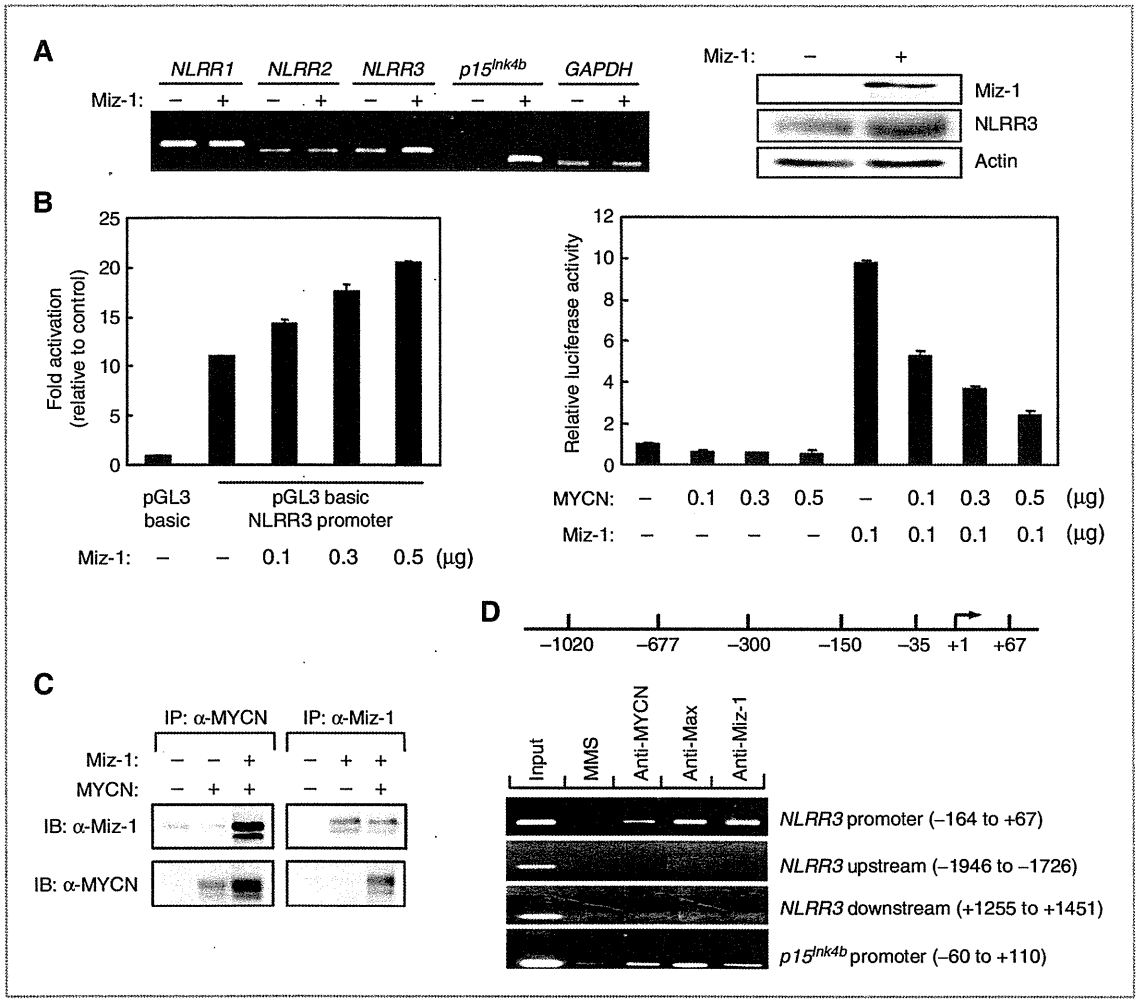


Figure 3. Regulation of the *NLRR3* promoter by MYCN and Miz-1. A, left, RT-PCR analysis showing expression of *NLRR1*, *NLRR2*, *NLRR3*, and $p15^{INk4b}$ in SH-SY5Y cells transiently transfected either with control or Miz-1–expressed plasmid. *GAPDH* was used as an internal control. Right, Western blot showing expression of *NLRR3* and *Miz-1* in SH-SY5Y cells transiently transfected either with control vector or with Miz-1 expressing vector. Actin was used as a loading control. B, left, Miz-1 enhances promoter activity of *NLRR3* in transient transfection assay. Data represent fold activation of the *NLRR3* promoter (−677 to +67) construct upon coexpression of increasing amounts of the expression plasmid for Miz-1 in SY5Y cells. Forty-eight hours after transfection, the cells were lysed and their relative luciferase activities were measured. Firefly luminescence signal was normalized on the basis of *Renilla* luminescence signal. Right, expression of MYCN reduces the basal activity of the *NLRR3* promoter and abrogates transactivation by Miz-1. SH-SY5Y cells were transiently cotransfected with or without constant amount of the expression plasmid for the Miz-1 and 0.1 μg of *NLRR3* promoter (−677 to +67) together with or without the increasing amounts of the expression plasmid for MYCN. The luciferase activity was determined as in B, left. Results are the mean of 3 independent experiments ± SD. C, interaction between MYCN and Miz-1 in NBL cells. Whole cell lysates prepared from SK-N-AS cells transfected with indicated vectors and immunoprecipitated (IP) with the monoclonal anti-MYCN antibody or with polyclonal anti–Miz-1 antibody. The immunoprecipates were analyzed by immunoblotting (IB) with the polyclonal anti–Miz-1 antibody or with monoclonal anti-MYCN antibody, respectively. D, ChIP analysis of SH-SY5Y cells was carried out by using the indicated antibody and PCR primers specific for the different part of *NLRR3* promoter (top 3 panels), upstream, downstream (middle 2 panels) regions of the *NLRR3* gene, and for $p15^{INk4b}$ promoter (bottom).

and *NLRR2*, showed no change. The increased expression of NLRR3 protein was also confirmed by Western blot analysis (Fig. 3A, right). This induction of NLRR3 by Miz-1 was also observed in SK-N-AS cells (Supplementary Fig. S3). To determine whether Miz-1 activates the *NLRR3* promoter, the region spanning exon 2 and 5′-upstream sequences of the *NLRR3* gene (nucleotide −1,020 to +67) was cloned and analyzed for promoter activity by using a luciferase reporter assay. The promoter deletion analysis showed that a nucleotide position between −677 and +67 gives maximum promoter activity (Supplementary Fig. S4A). The core promoter region (−35 to +67) also